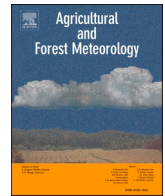


Contents lists available at [ScienceDirect](https://www.sciencedirect.com)

Agricultural and Forest Meteorology

journal homepage: www.elsevier.com/locate/agrformet

Gross primary production (GPP) and red solar induced fluorescence (SIF) respond differently to light and seasonal environmental conditions in a subalpine conifer forest

Julia C. Yang^{a,*}, Troy S. Magney^b, Loren P. Albert^c, Andrew D. Richardson^d, Christian Frankenberg^{e,f}, Jochen Stutz^g, Katja Grossmann^h, Sean P. Burns^{i,j}, Bijan Seyednasrollah^d, Peter D. Blanken^j, David R. Bowling^a

^a University of Utah, School of Biological Sciences, Salt Lake City UT 84112, USA

^b University of California, Davis, Department of Plant Sciences, Davis, CA 95616, USA

^c West Virginia University, Department of Biology, Morgantown, WV 26505, USA

^d Northern Arizona University, Center for Ecosystem Science and Society, and School of Informatics, Computing, and Cyber Systems, Flagstaff, AZ 86011, USA

^e California Institute of Technology, Division of Geological and Planetary Sciences, Pasadena, CA 91125, USA

^f NASA Jet Propulsion Laboratory, California Institute of Technology, Pasadena, CA 91125, USA

^g University of California, Los Angeles, Atmospheric and Ocean Sciences, Los Angeles, CA 90095, USA

^h University of Heidelberg, Institute of Environmental Physics, 69120, Heidelberg, Germany

ⁱ National Center for Atmospheric Research, Boulder, CO 80301, USA

^j University of Colorado, Department of Geography, Boulder, CO 80309, USA

ARTICLE INFO

Keywords:

solar induced fluorescence
artificial neural network
light response curves
phenology
conifer forest
eddy covariance flux

ABSTRACT (3 0 0 W O R D S)

The phenology of montane conifer forests is likely to shift in response to climate change and altered seasonal dynamics of light, temperature, and moisture. Solar-induced fluorescence (SIF) is expected to provide substantial improvement for mapping temporal changes in evergreen gross primary production (GPP) over greenness-based remote sensing indices. The utility of SIF to monitor seasonal changes in the phenology of conifer photosynthesis depends on the degree to which GPP and SIF respond in synchrony to key environmental drivers. However, to what extent SIF and GPP become decoupled by responding differently to the combined effects of light and other environmental conditions remains unknown. The goal of this study was to characterize the responses of GPP and SIF_{red} to a suite of environmental drivers at the half-hour time scale and determine how these relationships change across seasons. We analyzed one year of tower-based SIF_{red} and eddy covariance-derived GPP data from a conifer forest at Niwot Ridge, Colorado. We compared the light responses of GPP and SIF_{red} across the year, finding that SIF_{red} increased in response to light earlier in the year than did GPP. The light response of GPP had a positive temperature dependence in spring, and this dependency reversed in summer due to increased evaporative demand, while the light response of SIF_{red} was less temperature dependent. Using artificial neural network ensemble analysis, we found that from spring to summer, SIF_{red} did not exhibit a parallel response to the seasonally dynamic temperature and moisture controls on GPP. In summer SIF_{red} was not correlated with canopy conductance, suggesting that SIF is less sensitive to stomatal control than GPP. Our results suggest that, in conifers, photosystems begin to activate in spring prior to when water becomes available for photosynthesis, presenting a challenge for the use of SIF as a phenological indicator in conifer forests.

Introduction

Improving our ability to monitor how carbon (C) dynamics of the terrestrial biosphere interact with climate is critical for studying the

function of ecosystems now and in the future. A complete understanding of the terrestrial C cycle depends on our ability to quantify seasonal change in photosynthetic function, and how this is correlated with environmental conditions across time. Although estimating the timing

* Corresponding author:

E-mail address: julia.yang@utah.edu (J.C. Yang).

<https://doi.org/10.1016/j.agrformet.2022.108904>

Received 22 June 2021; Received in revised form 1 March 2022; Accepted 7 March 2022

Available online 12 March 2022

0168-1923/© 2022 Elsevier B.V. All rights reserved.

and magnitude of terrestrial gross primary productivity (GPP) has been a major goal of Earth system science for decades (Beer et al., 2010; Piao et al., 2013; Smith et al., 2016), major uncertainties persist, and it remains an ongoing challenge for ecologists to provide high-quality GPP estimates in uncontrolled field settings (Ryu et al., 2019).

A traditional method of estimating GPP is the light use efficiency (LUE) model (Monteith, 1977, 1972), which relies on the relationship between absorbed light and carbon uptake. The LUE model has been the paradigm in remote sensing to evaluate GPP on ecosystem to global scales (Field et al., 1995; Hilker et al., 2008; Running et al., 2004) and can be expressed as:

$$APAR = fAPAR * PAR$$

$$GPP = APAR * LUE$$

where LUE is the light use efficiency of CO₂ assimilation (Gitelson & Gamon, 2015), and APAR is the photosynthetically active radiation (PAR) absorbed by green leaves: equal to the total amount of PAR times the fraction absorbed by the canopy (fAPAR). Typically, reflectance indices related to leaf chlorophyll content and canopy structure (i.e. canopy 'greenness'), such as the normalized difference vegetation index (NDVI) or enhanced vegetation index (EVI), have been used to estimate changes in the fAPAR term (Goward and Huemmrich, 1992; Myneni and Williams, 1994; Sellers, 1985; Tucker, 1979; Viña and Gitelson, 2005), while adjustments for LUE are made based on its parameterized response to meteorological data (Running et al., 2004). However, NDVI and EVI do not adequately reflect temporal changes in plant function in evergreen systems, where photosynthetic dynamics are not controlled by seasonal shifts in chlorophyll content or canopy structure (Gamon et al., 1995; Magney et al., 2019; Smith et al., 2019; Springer et al., 2017; Walther et al., 2016; Wong et al., 2019). Therefore, improved remote sensing methods that accurately monitor C fluxes in response to environmental variability are needed; in order to predict changes in conifer forests, and to enhance the accuracy of terrestrial biosphere models.

Because evergreen species retain needles throughout the year, changes in LUE are controlled by a variety of photoprotective processes (Björkman and Demmig-Adams, 1995) working in coordinated response to seasonal shifts in the environment. Winter dormancy is typically characterized by downregulation of photosynthesis and upregulation of *sustained* nonphotochemical quenching (NPQ) – photoprotective thermal dissipation processes that are retained overnight (Verhoeven, 2014). Spring activation involves upregulation of photosynthesis, and a transition from mostly *sustained* to primarily *reversible* forms of NPQ—thermal dissipation involving the xanthophyll cycle that responds rapidly to the environment (Demmig-Adams and Adams, 2006). These seasonal changes in photosynthetic regulation are driven by environmental controls including temperature, photoperiod, soil moisture, snow cover, and freeze/thaw cycles (Bauerle et al., 2012; Bowling et al., 2018; Ensminger et al., 2008; Goulden et al., 2012; Parazoo et al., 2018; Polgar and Primack, 2011; Way et al., 2017). Seasonal transitions depend on the interactions between these environmental cues and physiological mechanisms that are site- and species-specific, and neither models nor greenness indices reliably predict photosynthetic phenology of coniferous evergreens (Chang et al., 2019; Frechette et al., 2015; Parazoo et al., 2018; Richardson et al., 2012; Turner et al., 2005).

The subtle seasonal variation of fAPAR and persistent greenness of conifer forests makes it difficult to study seasonal changes in photosynthetic function. For this reason, the remote sensing of chlorophyll fluorescence, termed solar-induced fluorescence (SIF), has received significant attention over the last decade as an improved method of measuring productivity (for review see Mohammed et al., 2019). When a leaf absorbs light, some of the energy is used to drive the photochemical reactions of photosynthesis, a portion is dissipated as heat via NPQ, and a small fraction (< 2%) is re-emitted by chlorophyll as fluorescence

(Maxwell and Johnson, 2000), with wavelengths from 640 nm – 850 nm. Because fluorescence emission is linked to the light reactions of photosynthesis (Gu et al., 2019), it is sensitive to both APAR and photochemical efficiency. Therefore, in theory SIF is linked to the photosynthetic function of leaves rather than simply green pigment content or leaf area (Gu et al., 2019; Porcar-Castell et al., 2014; Yang et al., 2015), and numerous studies confirm that SIF carries novel information on the dynamics of photosynthesis compared with previous remote sensing indices (Frankenberg et al., 2011b; Guanter et al., 2012; Joiner et al., 2011; Magney et al., 2019).

From canopy to global scales, SIF has been shown to display a linear association with GPP across biomes (e.g Li et al., 2018.; Sun et al., 2018, 2017; Wood et al., 2017; Yang et al., 2015). To some degree SIF is related to GPP due to their shared response to APAR, as has been shown in crops (Dechant et al., 2020; Miao et al., 2018; Wu et al., 2020; Yang et al., 2018; P. Yang et al., 2020) and grasslands (Smith et al., 2018). On the other hand, SIF correlates to seasonal changes in photoprotective pigments and photochemical efficiency in evergreen systems that exhibit little variation in APAR (Magney et al., 2019). In contrast to the often-reported linear association between SIF and GPP by remote sensing studies, at the leaf scale there is a nonlinear relationship between fluorescence emission and C assimilation (Flexas et al., 2002; Gu et al., 2019; Magney et al., 2020), as net assimilation saturates under high light while fluorescence continues to increase. Measures of SIF from remote sensing platforms and GPP derived from eddy covariance (EC) flux measurements of net ecosystem exchange (NEE) both integrate across the structural and physiological variability of the individual leaves that compose a canopy. As spatiotemporal scales become coarser, this integration averages out the nonlinearities in the SIF-GPP relationship (Magney et al., 2020; Y. G. Zhang et al., 2016). The fact that SIF is not a perfect representation of GPP does not negate its usefulness, rather, we need to know under what environmental conditions is SIF a 'reasonable' proxy for photosynthesis (Magney et al., 2020).

Advancement in our understanding of SIF is expected to provide a significant improvement in our ability to model productivity of terrestrial ecosystems (Frankenberg et al., 2014; Guanter et al., 2014; Parazoo et al., 2014; Verrelst et al., 2016), however, the use of SIF as a phenological predictor of GPP seasonality in conifer forests warrants further study. If we accept the premise that the link between SIF and GPP at increasing scales is due, in part, to their shared response to APAR (Miao et al., 2018; Yang et al., 2018), SIF and GPP should be nonlinearly related when plant physiological response to environmental conditions causes SIF and GPP to respond differently to light. Recently, Kim et al. (2021) showed that in autumn a non-linear SIF-GPP relationship was associated with differences between the light responses of SIF and GPP, and we expect this to be true across seasons. In addition, the GPP-SIF relationship may be modified by environmental controls (Chen et al., 2021; Wieneke et al., 2018; Wohlfahrt et al., 2018) and vary across ecosystems, therefore further research is needed to investigate whether the impacts of complex environmental interactions on GPP are also captured by SIF. These issues motivated us to investigate potential differences in the response of GPP and SIF to light and other environmental factors.

We analyzed one year of continuous canopy-scale red SIF (SIF measured from 680 nm -686 nm wavelength, SIF_{red}) and EC GPP data in a subalpine conifer forest at Niwot Ridge CO, USA. Previously, Magney et al. (2019) demonstrated that SIF closely followed changes in photosynthetic capacity from hourly to weekly time scales in this forest. We expand on the former study by further investigating the responses of half-hourly SIF_{red} and GPP to the combined effects of light and weather, and how these relationships change across seasons. To do this, we first focus on the light responses of GPP and SIF_{red}, then continue with an artificial neural network (ANN) ensemble analysis. We ask: Q1) when are there fundamental differences in the light responses of SIF_{red} and GPP; and Q2) when and how do SIF_{red} and GPP differ in their response to environmental controls?

Methods

Study Site

We analyzed data during the year 2018 from a high elevation (3050 m) subalpine conifer forest at Niwot Ridge, Colorado, USA (an AmeriFlux Core Site, 40.03°N, 105.55°W). The site is composed of lodgepole pine (*Pinus contorta* Douglas ex Loudon), Engelmann spruce (*Pinus engelmannii* Parry ex Engelm.), and subalpine fir (*Abies lasiocarpa* (Hook.) Nutt.). The tree density near the tower is ~4000 trees ha⁻¹, canopy height is 12–13 m, and leaf area index is 3.8–4.2 m² m⁻² (Burns et al., 2015). The understory is sparse, with few tree seedlings and patches of *Vaccinium myrtillus* (~25% cover, Monson et al., 2002). Mean annual temperature is 1.5°C and mean annual precipitation 800 mm, with ~65% falling as snow and a persistent snowpack from November to May (Monson et al., 2005). We refer the reader to earlier publications for detailed site description (Bowling et al., 2018; Burns et al., 2015; Monson et al., 2002, 2005). Needles at this site remain green year-round, and previous studies have shown conclusively that there is

little seasonal change in APAR, NDVI, or needle chlorophyll concentration (Bowling et al., 2018; Magney et al., 2019). For the year 2018 of the present study, annual cumulative precipitation was 412 mm (~50% of average), and annual cumulative GPP was 678 g C m⁻², which is 88% of the average from 1999–2012 (767 ± 45 g C m⁻²; Knowles et al., 2015). These data indicate that the forest experienced drought during the study year.

Eddy covariance and meteorological data

We measured net ecosystem exchange of CO₂ (NEE) from the flux tower using a sonic anemometer (CSAT3; Campbell Scientific) and closed-path infrared gas analyzer (model LI-6262; LI-COR Biosciences) at 21.5 m height. Downwelling photosynthetic photon flux density (PPFD, LI-COR 190-SA), net radiation (R_n, REBS Q-7.1), latent heat flux (LE, CSAT3), sensible heat flux (H, CSAT3), air temperature (T_{air}, Vaisala HMP-35D), wind speed (U, CSAT3), and friction velocity (u*, CSAT3) were measured above canopy (21.5 m). Vapor pressure saturation deficit of air (VPD, Vaisala HMP-35D) was measured at 8m

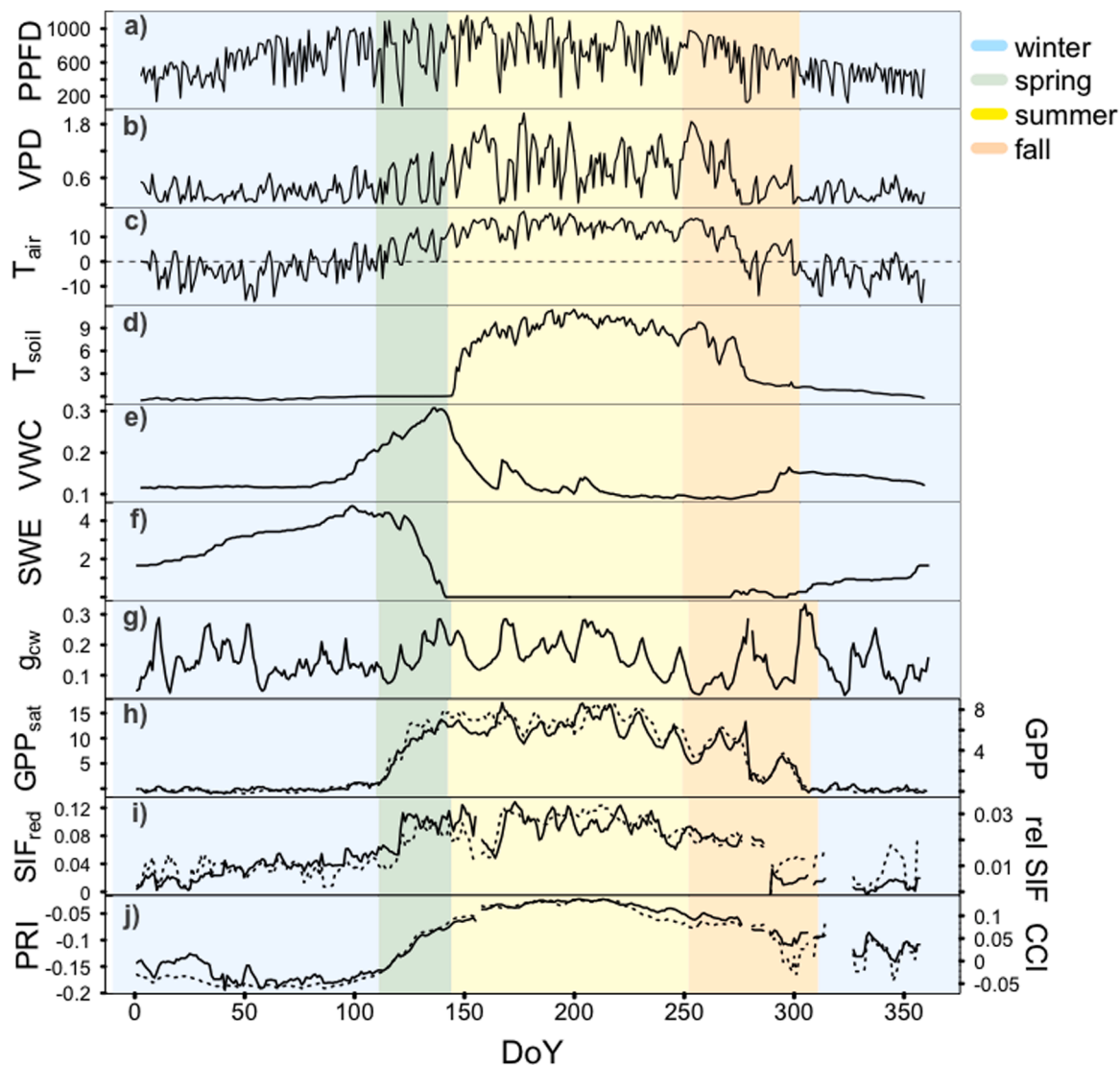


Fig. 1. Annual course of environmental variables for 2018, plotted as daytime means of a) photosynthetic photon flux density—PPFD ($\mu\text{mol m}^{-2} \text{s}^{-1}$), b) vapor pressure deficit—VPD (kPa), c) air temperature— T_{air} ($^{\circ}\text{C}$), d) soil temperature— T_{soil} ($^{\circ}\text{C}$), e) soil volumetric water content—VWC ($\text{cm}^3 \text{cm}^{-3}$), and f) snow water equivalent—SWE (cm). g) Five-day moving average of canopy conductance— g_{CW} ($\text{mol m}^{-2} \text{s}^{-1}$). h) Daily forest photosynthetic capacity— GPP_{sat} (solid line; $\mu\text{mol CO}_2 \text{m}^{-2} \text{s}^{-1}$), and five day moving average of GPP (dashed line; $\mu\text{mol CO}_2 \text{m}^{-2} \text{s}^{-1}$). Five-day moving average of i) SIF_{red} (solid line; $\text{mW m}^{-2} \text{nm}^{-2} \text{sr}^{-1}$) and relative SIF_{red} (dotted line, unitless), and j) the photochemical reflectance index—PRI (unitless) and the chlorophyll carotenoid index—CCI (dashed line; unitless). Data were visually divided into winter, spring, summer, and fall based on GPP_{sat} , shown in blue, green, yellow, and orange, respectively

height, soil heat flux (Q , REBS HFT-1) at 0-10cm depth, and barometric pressure (P_{bar} , Vaisala PTB-101B) at 12 m height. At 5 cm depth in mineral soil we measured soil temperature (T_{soil}) using a thermistor probe (CS107, Campbell Scientific), and soil moisture (volumetric water content, VWC), which was taken as the average of twelve water content reflectometers (CS616 & CS615, Campbell Scientific). We used data from these twelve sensors at 5 cm depth to account for horizontal spatial heterogeneity (Fig. S1a). We note that VWC data from 5cm depth may not represent water available to trees at different rooting depths, however data from VWC sensors at different depths in a profile located a few meters from the nearest bole showed that the 5cm data were reasonably representative of soil moisture to a depth of 30cm at this site (Fig. S1b). For detailed sensor description, see Burns et al. (2015). For all flux and meteorological data we used daytime half-hourly averages, where daytime was defined as PPFD $> 5 \mu\text{mol m}^{-2} \text{s}^{-1}$. Daily snow water equivalent (SWE) data were provided by the USDA/Natural Resources Conservation Service Snow Telemetry Network (SNOTEL) site located approximately 400 m from the tower.

We partitioned GPP from NEE using both the nighttime (Reichstein et al., 2005) and daytime (Lasslop et al., 2010) methods using the REdyProc R package (Wutzler et al., 2018). The GPP data presented in the primary text are from the nighttime partitioning method, while differences due to the daytime partitioning method are discussed in the supplement (S5). Seasons were determined visually based on a time-varying index of photosynthetic capacity, which we define as the light saturated rate of GPP (GPP_{sat} ; Bowling et al., 2018), shown in Fig. 1h. GPP_{sat} can be thought of as the ecosystem scale analog of leaf-level photosynthetic capacity (A_{max}). We determined GPP_{sat} according to Bowling et al. (2018) by fitting hyperbolic light-response-curves in a 5-day moving window to the equation $GPP = \alpha \cdot \text{PPFD} / (b + \text{PPFD})$, and then calculating GPP at a light saturated level of PPFD ($2000 \mu\text{mol m}^{-2} \text{s}^{-1}$) as $GPP_{sat} = \alpha \cdot 2000 / (b + 2000)$.

In order to compare the sensitivities of GPP and SIF to stomatal control, we calculated canopy conductance to water vapor g_{cw} , which is the ecosystem scale analog of stomatal conductance, according to Blanken et al. (1997):

$$\frac{1}{g_{cw}} = \frac{1000c_p VPD\rho}{\gamma LE} - r_a$$

where aerodynamic resistance r_a is calculated according to Verma (1989):

$$r_a = \frac{U}{u^*{}^2} + \frac{2.5}{u^*}$$

and c_p is the specific heat of air at constant pressure, ρ is the air density calculated from barometric pressure (P_{bar}) and air temperature (T_{air}), and $\gamma = (P_{bar} * c_p / .622 * \lambda)$, where λ is the latent heat of vaporization of water calculated from T_{air} .

Tower-based SIF

SIF was measured continuously at 26-m height with a PhotoSpec spectrometer system (Grossmann et al., 2018) mounted at the top of the flux tower. SIF was retrieved using the in-filling of Fraunhofer line depth (Plascyk and Gabriel, 1975), using full spectral fitting techniques in spectral windows devoid of telluric absorption features (e.g Frankenberg et al., 2011a.). A failure of our far-red spectrometer led to large data gaps in the far-red region, therefore we used SIF_{red} (680-686 nm) only. The PhotoSpec consists of a 2D scanning telescope unit with a 0.7° field of view. The instrument collected data in elevation scans from nadir to the horizon in 0.7° steps at a fixed azimuth angle in the north-northeast direction. By taking zenith scans at a fixed azimuth angle rather than nadir measurements, PhotoSpec field of view captured all species in this ecosystem, therefore these data are a reasonable representation of the species present in the EC footprint. During the scanning routine, diffuser

spectra were taken every 3 minutes. We filtered the SIF_{red} data for when NDVI was > 0.6 , when the solar zenith angle was $< 90^\circ$, and the viewing zenith angle $< 30^\circ$ to avoid retrievals coming from the soil, snow, or low solar/viewing zenith angles. These decisions are consistent with Magney et al. (2019), and were chosen to be as conservative as possible. In addition, we used Phenocam images (Richardson, 2019) to exclude periods with snow on the canopy. We then averaged data from all scans on a half-hourly basis ($n > 5$ observations) to match the temporal resolution of flux tower data.

Radiative transfer and canopy structure are important determinants of variation in SIF, including at the seasonal scale (Dechant et al., 2020; Liu et al., 2020; Yang and van der Tol, 2018; Zeng et al., 2019), and continuously changing solar-view geometry imposes directional effects on the fluorescence signal (Biriukova et al., 2020; Zhang et al., 2018). Because data were taken along a fixed azimuth angle that pointed north-northeast, throughout the day the canopy in the scan path experienced different fractions of sun and shade. In other words, some fields of view might be shaded in the morning, while in the evening – at equivalent PAR – they might be sunlit. Canopy shading effects were unavoidable, and rather than excluding data by introducing a bias towards sunlit conditions, we chose to maintain the full dataset in order to represent canopy average illumination as would be represented in the EC flux footprint.

To test the effects of illumination geometry, we calculated a relative SIF (Fig. 1i; Magney et al., 2019; Pierrat et al., 2021) which was normalized by red reflected radiance from the retrieval window (680 nm - 686 nm): $relative\ SIF_{red} = SIF_{red} / \rho_{Red_{680-686}}$. Relative SIF_{red} exhibited little variation in response to light (Fig. S2), indicating that the light response of SIF was not biased due to diurnal variation in illumination conditions. Additionally, we note that SIF_{red} is subject to stronger reabsorption affects by chlorophyll than SIF_{far-red}, and these reabsorption effects may be exacerbated by the previously mentioned geometry issues and impact our measurements on the diurnal time scale. However, Magney et al. (2019) determined that there was no discernable difference between red and far-red SIF for tracking GPP in this dataset, and showed that red and far-red SIF scale linearly across the seasons in this ecosystem on hourly-weekly timescales. The annual time course of SIF_{red}, relative SIF_{red} are shown alongside the environmental data in Fig. 1.

The photochemical reflectance index (PRI) is related to de-epoxidation of xanthophyll pigments (*reversible* NPQ) in the short term, which reduces reflectance at 531 nm (Gamon et al., 1992), while on the seasonal scale the PRI signal is dominated by changes in chlorophyll:carotenoid ratios (Porcar-Castell et al., 2012; Wong et al., 2020; Wong and Gamon, 2015a). The chlorophyll:carotenoid index (CCI) is useful for studying changes in pigment ratios that occur on a seasonal scale (Gamon et al., 2016). We measured PRI and CCI (Fig. 1j) to give an indication of photoprotective pigment-related biological controls on the photosynthetic seasonality in our ANN analysis. The same PhotoSpec instrument used to calculate SIF provides moderate resolution spectral reflectance data (Grossman et al., 2018), which were used to calculate PRI and CCI as:

$$PRI = (\rho_{569:571} - \rho_{520:532}) / (\rho_{568:571} + \rho_{520:532})$$

$$CCI = (\rho_{409:415} - \rho_{735:745}) / (\rho_{409:415} + \rho_{735:745})$$

where $\rho_{nm:nm}$ is the average reflectance across the wavelength range in nm (Gamon et al., 1992). When aggregated to the daily scale, PRI and CCI exhibited a very similar annual time course (Fig. 1j) as expected. Sun sensor geometry effects complicate the acquisition of PRI (Hall et al., 2008), thus a limitation of our study is that data obtained with a single sensor are not robust enough to thoroughly account for these illumination complexities.

Artificial Neural Networks

Monitoring data in uncontrolled field settings does not distinguish the partial effects of any single environmental or climatic variable such as one might obtain through a controlled experiment (Kolari et al., 2014), and even then, feedbacks between variables make full separation of effects difficult or impossible. As a result, model-based analyses of observational data commonly rely on functional relationships specified a priori (e.g., Lasslop et al., 2010). Instead, we used an ensemble of ANNs to identify the hierarchy of environmental controls of GPP and SIF_{red} and derive their functional relationships directly from the observations, without making assumptions about the shape of each response (Albert et al., 2017; Moffat et al., 2010). ANNs are non-parametric empirical models that are useful for extracting nonlinear functional relationships from noisy, multivariate datasets, and often outperform other semi-empirical or process-based models (Moffat et al., 2010; Abramowitz, 2005; Keenan et al., 2012). In brief, an ANN model identifies correlations between controlling input variables (drivers) and the responding output variable(s) at the time scale of the data during a model training process (Moffat et al., 2010). Previous papers describe ANNs and their applications in greater depth (see Albert et al., 2017; Bishop, 1995; Lek and Guégan, 1999; Moffat et al., 2010; Olden et al., 2008; Papale and Valentini, 2003).

To evaluate the responses of GPP and SIF_{red} to variation in seasonal environmental conditions, we used an ensemble of feedforward ANNs trained by backpropagation using Matlab's neural network toolbox (Beale et al., 2014; Bishop, 1995; Rojas, 1996). Each ANN model structure consisted of an input layer with n nodes, where n = number of candidate driver(s) (independent variables), which fed into a five-node hidden layer, whose outputs then fed into the target layer (response variable, GPP or SIF_{red}). Data moved in the forward direction using a sigmoid activation function, with each node interconnection assigned a weight during training that determines the behavior of the network.

Data were randomly divided into three subsets for training (60%), testing (20%), and validation (20%). Only non-gap-filled data were used. Prior to training, candidate drivers were scaled from $[-1, 1]$ to be within the linear range of the sigmoid function output (Beale et al., 2014). In the ANN context, "drivers" represent independent variables, or the inputs of the network. Rather than the typical $[0,1]$ scaling, the response (GPP or SIF_{red}) was further limited inside the linear range and scaled to $[.3,.7]$ to reduce edge effects, which can have a large impact on the partial derivatives (see below, Moffat, 2012). During training, the relationship of the response variable with each candidate driver was taken directly from the data and mapped into the network. We trained each ANN ten times using the Levenberg–Marquardt algorithm, and determined the performance of each using the mean-square error from the testing subset. For robustness, we then used the ANN with the lowest mean squared error for our analysis (Moffat et al., 2010).

Using the ANN approach presented in Moffat et al. (2010) and Albert et al. (2017), we characterized a hierarchy of environmental controls of SIF_{red} and GPP separately and for each season. First the ANN was trained with all candidate drivers to produce a benchmark coefficient of determination (r^2) of the total explanatory capability of the data (see dashed line in Fig. 4). This indicates the maximum GPP or SIF_{red} variability explained by the candidate drivers, and the degree to which variability was unaccounted for due to either measurement noise and/or missing drivers (Moffat et al., 2010). Initial candidate drivers included: T_{air} , T_{soil} , VWC, VPD, precipitation, incoming PPFD, SWE, and PRI. The PRI was included as a variable under the assumption that it may be a proxy for xanthophyll pigment state on diurnal time scales (Gamon et al., 1992; Porcar-Castell et al., 2012; Zhang et al., 2016), and therefore is considered as a biological rather than environmental driver in this paper. We used PRI rather than CCI because the ANN identifies correlations at the time scale of the data, in this case half-hourly, during a model training process, and ANNs were trained within rather than across individual seasons. In addition, SIF_{red} was included as a candidate

driver for GPP, though we stress that it is not a "driver" in the sense that GPP is not controlled mechanistically by SIF . We did this to assess the relative explanatory power of SIF compared to other environmental predictors.

After determining the benchmark, we trained ANNs with each candidate driver individually and ranked them based on r^2 (see dark bars in Fig. 4) to quantify their importance. After the primary (most important) driver was identified, ANNs were trained with the primary driver, plus each additional candidate driver to determine any secondary drivers (see light bars in Fig. 4). The degree of network performance improvement that resulted from the addition of the secondary driver indicates the amount of new information that driver contributed beyond the primary driver. This strategy informs instances when the response was dominated by a certain driver, such as light, and the ANN may not have been able to pick up underlying minor correlations, such as temperature. Since ANNs with different single-inputs (or dual-inputs) can have similar performance, we tested for statistically significant differences in performance across single-driver ANNs (Fig. 4, white asterisks), and across dual-driver ANNs (Fig. 4, black asterisks), by comparing the correlation coefficients (r) after a Fisher r -to- z transformation (Fisher 1921; Albert et al., 2017). If the z -statistics of more than three drivers were not statistically different from each other ($p > 0.05$ for t -test), then no driver(s) were described as significantly primary or secondary. In cases where more than one candidate driver was tied for primary driver, the driver with the numerically highest r^2 was still used as the primary driver when determining secondary driver performance.

While the ANN rankings map the performance of the controlling drivers to the response, the numerical partial derivatives (PaD) of the network function further characterize the functional responses of GPP to changes in the drivers. The PaD with respect to each driver, PaD_i , represents the degree of change in GPP per measured physical unit. The partial derivative with respect to each input, $PaD_{i,j}$ (for $j = 1, \dots, N$ number of observations), was calculated following to Gevrey et al. (2003):

$$PaD_{j,i} = S_j \sum_{h=1}^{n_h} w_{ho} I_{hj} (1 - I_{hj}) w_{ih}$$

where S_j is the derivative of the output neuron, n_h is the number of neurons in the hidden layer, and for each h th hidden neuron, I_{hj} is the output of the hidden neuron, w_{ho} is the weight from the hidden to the output neuron, and w_{ih} is the weight from the input to the hidden neuron. To make comparisons across inputs with different units, we normalized the partial derivatives, *nor. PaD_{i,j}*, as in Moffat et al. (2010). Then we took the averages of all the negative normalized PaDs, *neg. PaD_i*, and all the positive normalized PaDs, *pos. PaD_i* (Moffat et al., 2010):

$$neg.PaD_i = \frac{1}{N} \sum_{PaD_{i,j} < 0} (nor.PaD_{i,j})$$

$$pos.PaD_i = \frac{1}{N} \sum_{PaD_{i,j} > 0} (nor.PaD_{i,j})$$

These positive and negative fractions of the partial derivatives were used to determine the sensitivity of the GPP response to changes in the candidate drivers and whether the effect was increasing or decreasing (Moffat et al., 2010).

Results & Discussion

Monthly light responses of SIF_{red} and GPP

Over recent years, many studies have demonstrated a linear relationship between SIF and GPP, derived across an entire season at large spatiotemporal scales (e.g Li et al., 2018.; Sun et al., 2018). If SIF emission is proportional to GPP, we would expect that they share a

similar response to variation in light. Therefore, we compared the light response of GPP with the light response of SIF_{red} for each month of the year (Fig. 2). To avoid making assumptions about the shape of the curve, we fit a non-parametric generalized additive model (GAM) to each light response. We found that the light responses of SIF_{red} and GPP each varied across months of the year, but did so in different ways. SIF_{red} exhibited a response to light prior to the onset of GPP: there was a clear increase in SIF_{red} with increasing light as early as February and March, while the first occurrences of non-zero GPP were recorded in April (Fig. 2). These results suggest that photosystems become activated in spring (increasing SIF_{red}) ahead of when the EC method detects the onset of photosynthesis following winter dormancy. From May to September, GPP saturated under high PPFD while SIF_{red} continued to increase, as expected (Gu et al., 2019; Magney et al., 2020; Fig. 2,3). Saturation of GPP and linearity of tower-based SIF at high light agrees with patterns in Korean pine (Kim et al., 2020) and in C3 crops (He et al., 2020a).

That the onset of SIF_{red} occurred prior to GPP in spring is not surprising given the many complex factors that govern the phenological shift from winter photosynthetic downregulation to spring growing season. Rather than being simply ‘off’ one season and ‘on’ the next, conifer forests experience intermittent periods of activity in response to periods of favorable conditions (Pierrat et al., 2021). For example, photosynthetic activity has been observed in coniferous trees during warm winter days (Ensminger et al., 2004; Knowles et al., 2020; Sevanto

et al., 2006), but was not observed at Niwot Ridge where frozen boles limited water transport and precluded winter or early spring GPP despite favorable leaf temperature (Bowling et al., 2018). Furthermore, even when photosynthesis is absent indicating shutdown of the carbon reactions, leaf level fluorescence continues (Kolari et al., 2014; Ottander et al., 1995; van der Tol et al., 2014; Verhoeven, 2014), including at Niwot Ridge where Magney et al. (2019) reported small wintertime potential for electron transport from PAM fluorescence data.

Seasonal differences in the timescales on which the light and carbon reactions of photosynthesis are regulated result in a decoupling of the SIF -GPP relationship. A multitude of signaling pathways govern the transition of photosynthesis between down- and upregulated states, and the environmental and physiological controls of these pathways remain an active area of research (e.g Demmig-Adams et al., 2012.; Esteban et al., 2015; Kolari et al., 2014; Porcar-Castell, 2011; Wong et al., 2019). Maintenance of some capacity of the electron transport chain is necessary for NPQ processes which require a transmembrane pH gradient (Verhoeven, 2014), resulting in winter fluorescence emission when GPP is absent. In spring, SIF and GPP may be decoupled due to within-leaf recycling of respiratory CO_2 before bole thaw and stomatal opening (Bowling et al., 2018). The increased role of cyclic electron transport around photosystem I (PSI) as a springtime energy sink (Frechette et al., 2015) may decouple GPP from $SIF_{far-red}$, but likely does not impact SIF_{red} emitted primarily from photosystem II (PSII). In addition, the spring increase in chlorophyll/carotenoid pigment pool ratios, which leads to

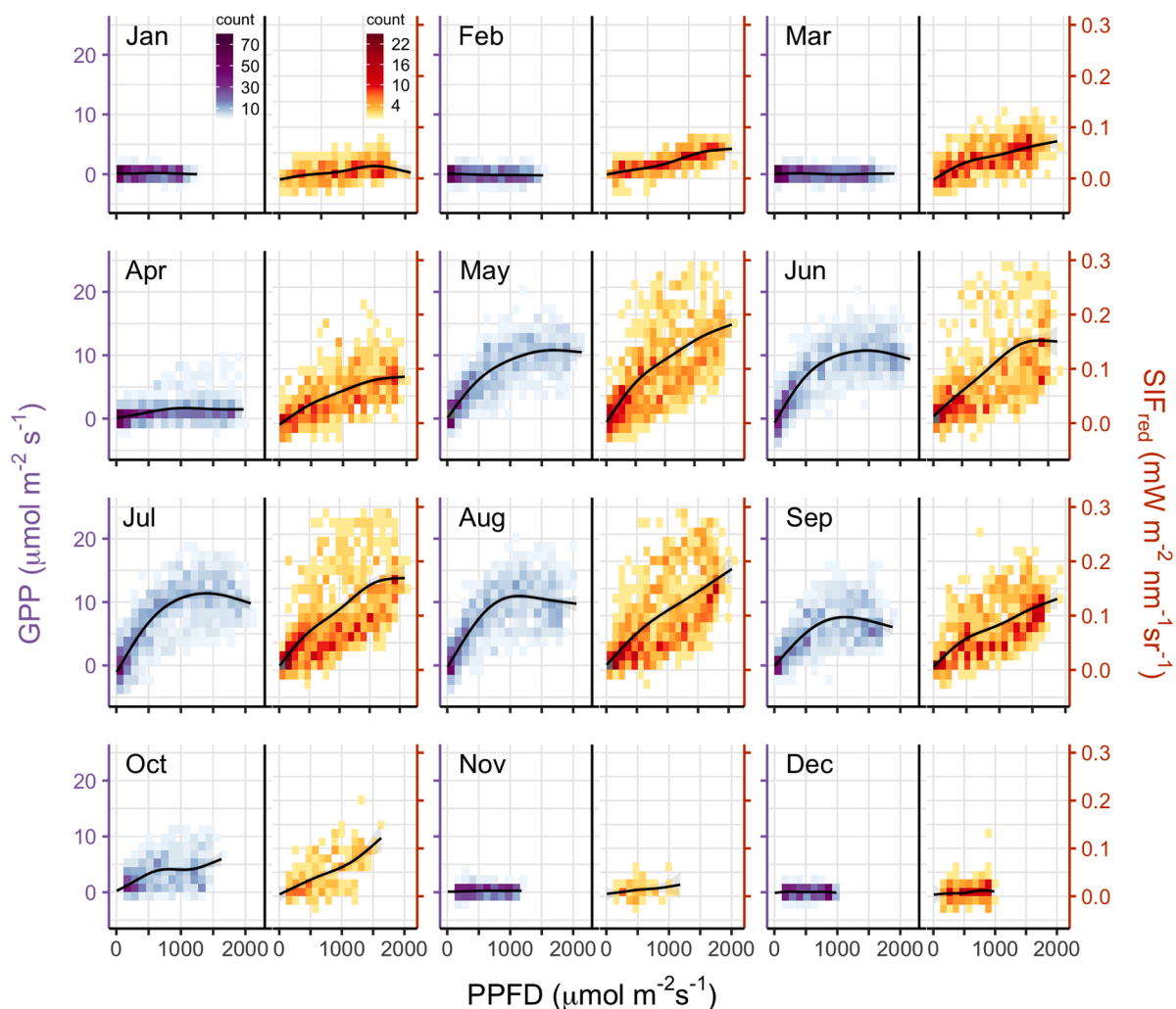


Fig. 2. The responses of GPP and SIF_{red} to sunlight (PPFD) for each month are shown side by side in blue and orange, respectively. Colors indicate bivariate frequency distributions as an indication of data density. Plotted lines are fits from a generalized additive model for each.

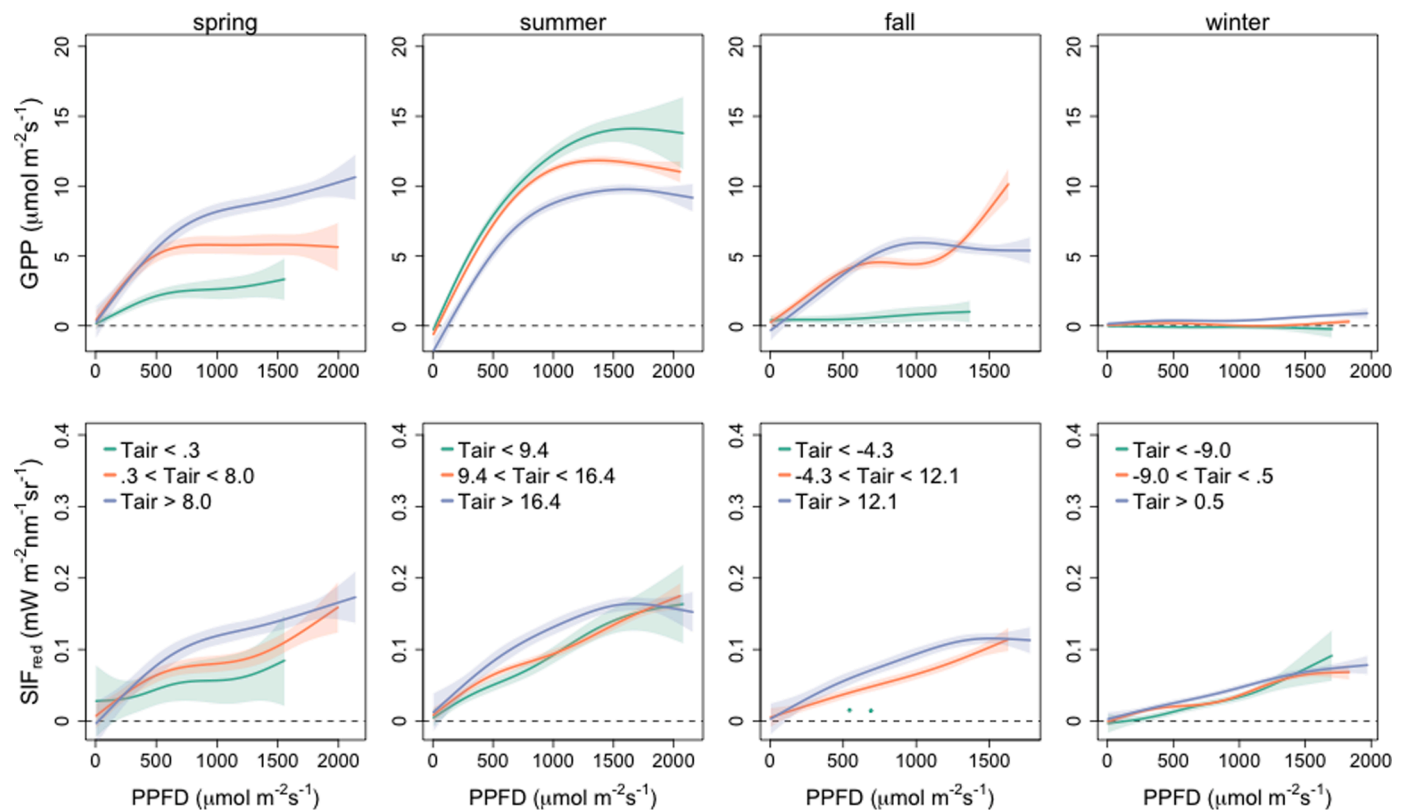


Fig. 3. Plotted lines are generalized additive model (GAM) fits with 95% confidence intervals. Each seasons' data is plotted in three temperature categories after splitting the range of temperature for that season into equal-sample-size thirds, with the coldest shown in green, mid-range in red, and warmest in blue. For the lowest temperature group in fall for SIF_{red} , insufficient data were available to produce a GAM fit, so the data are shown directly.

increasing photosynthetic activity and the transition from sustained to reversible NPQ (Wong et al., 2020), affects both SIF and GPP, but these effects may be decoupled in time (Fig. 1h,i,j). Thus, there is significant evidence for the decoupling between the light and carbon reactions of photosynthesis in winter and early spring in cold-acclimated evergreens. We hypothesize that these mechanisms are responsible for the seasonal decoupling of SIF_{red} and GPP observed in this study.

It is well established that there are significant limitations in using NDVI or EVI to map the phenology of evergreen photosynthesis, and it has been suggested that SIF may be an advancement over these traditional reflectance-based indices (Jeong et al., 2017; Walther et al., 2016). However, our finding that SIF_{red} varies with light prior to the onset of GPP presents a challenge for the use of SIF to predict the start of the growing season in conifer forests. In agreement, Parazoo et al. (2018) found that spring onset dates estimated from satellite SIF were up to one month earlier than dates estimated from EC flux towers in a boreal forest, and that this discrepancy would result in over 20% error in estimates of seasonal GPP (Parazoo et al., 2018). Although they partially attribute this finding to GOME-2 overpass time or monthly aggregation, our results provide new evidence that the differing responses of SIF and GPP to light contribute to the discrepancy in time between spring onset estimates. Thus, our results provide important information that SIF may not be a reasonable proxy for GPP during early spring, and under saturating light in summer.

Seasonal light responses of SIF_{red} and GPP

The annual course of GPP_{sat} was visually examined alongside temperature and moisture and used to divide the year into winter, spring, summer, and fall seasons (Fig. 1). Based on this GPP_{sat} seasonal classification, spring onset began after initiation of snowmelt and initial increase in soil VWC, while coinciding with the first sustained increase in

$T_{air} > 0^{\circ}C$ (Fig. 1). There was a marked increase in CCI during the spring onset (Fig. 1j). The end of spring was defined as the plateau in GPP_{sat} and coincided with the end of snowmelt. The start of the fall season was less clearly defined and was marked by generally declining yet highly variable GPP_{sat} and T_{soil} . Winter was defined by zero GPP_{sat} , sustained $T_{air} < 0^{\circ}C$, and stable T_{soil} (Maurer and Bowling, 2014).

While it is well established that light is important for driving the SIF-GPP relationship, photosynthesis also responds strongly to temperature (Huxman et al., 2003; Monson et al., 2005; Sage and Kubien, 2007; Albert et al., 2017). Therefore, we investigated how the sensitivities of GPP and SIF_{red} to light varied due to temperature across seasons (Fig. 3). We divided the data within each season based on the distribution of measured air temperature, into 3 groups of equal thirds (tertiles of T_{air}). We chose T_{air} because when the ANN was run with data from all seasons combined, T_{air} was the primary driver of GPP (data not shown), and T_{air} is commonly used to parameterize land surface phenology models (Richardson et al., 2006; Wu et al., 2012). The light response of GPP had a strong positive temperature dependence in spring (higher light-saturated GPP with higher T_{air}), and this pattern reversed in summer (lower light-saturated GPP with higher T_{air} , Fig. 3). Higher temperature in spring was associated with greater LUE (slope of the linear portion of the GPP curve), while in summer LUE did not vary with temperature (Fig. 3). In contrast, the light response of SIF_{red} was less temperature dependent in spring and did not exhibit the reversal in summer.

The reversal in temperature dependency of GPP from spring to summer suggests 1) there was a shift from temperature limitation to moisture limitation of photosynthesis, as higher temperature led to increased evaporative demand (higher VPD) and stomatal closure; and/or 2) summer T_{air} ($9.4 - 16.4^{\circ}C$) exceeded the photosynthetic temperature optima in these species ($\sim 10^{\circ}C$, Huxman et al., 2003). In support of the former, we found that VPD strongly influenced the light response

of GPP in summer, with lower light-saturated GPP under increased evaporative demand (Fig. S3), and this corresponded with a VPD dependence on the light response of canopy conductance (Fig S4). This provides evidence that SIF may be less sensitive to temperature,

evaporative demand and associated stomatal closure than GPP. In contrast with our results, Kim et al. (2020) found that the slope of the SIF-APAR relationship increased gradually with air temperature, while the slope of the GPP-APAR relationship did not change. The discrepancy

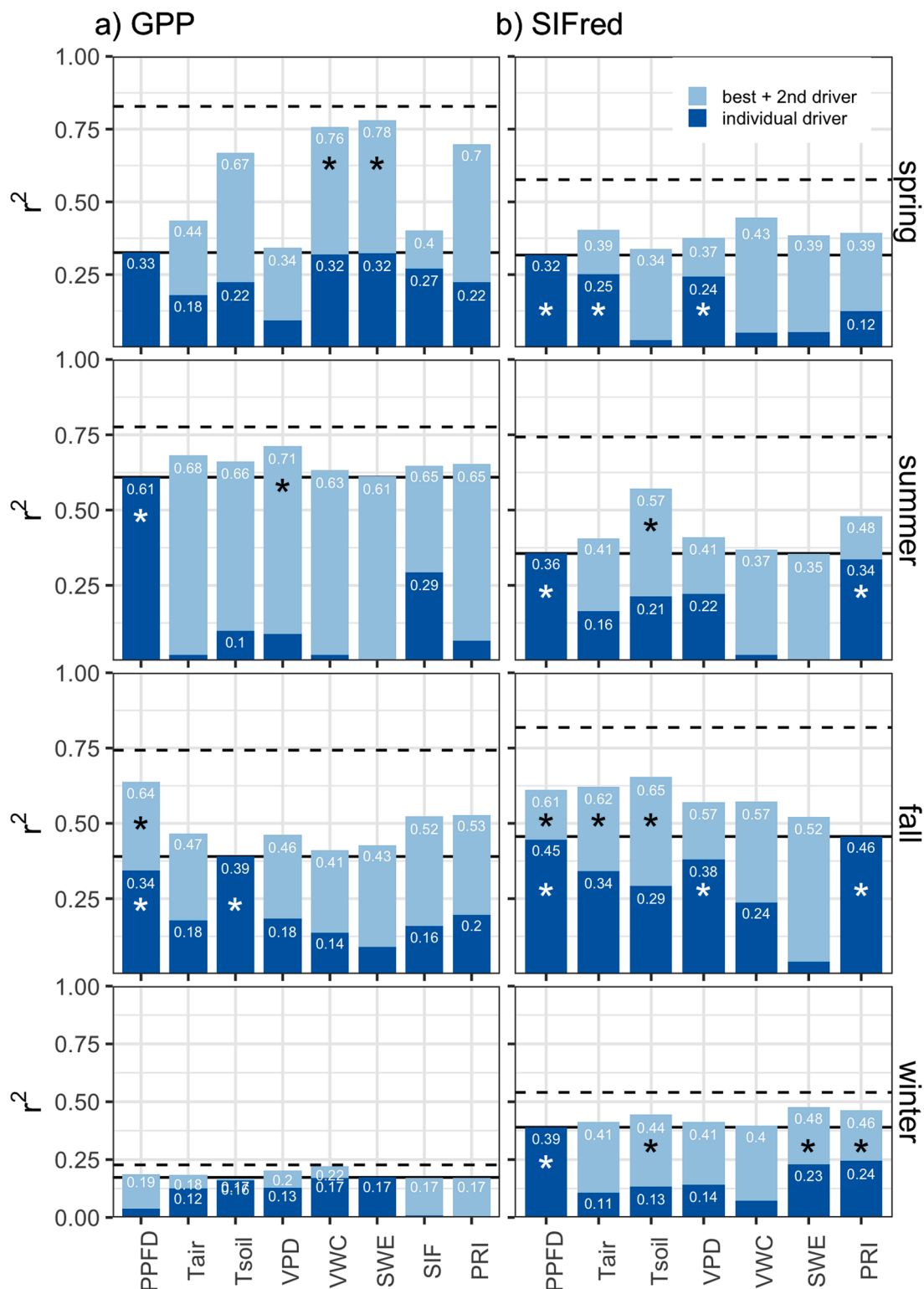


Fig. 4. Results from artificial neural network (ANN) analysis of potential environmental drivers of GPP and SIF_{red}. Dark bars represent the ANN performance run with each variable as a single input to the ANN. Light bars represent the ANN performance run with the top performing variable (PPFD in all cases except winter and fall GPP) plus one additional input variable. White and black asterisks represent the top performing primary and secondary input(s), respectively, after a Fisher r-to-z transformation. Solid black horizontal line indicates performance with the best primary driver, and light bars extension beyond this indicates improvement to the model upon addition of secondary input. Dashed horizontal line indicates benchmark performance of the model.

between these two studies is likely a result of their focus on autumn only, compared with our four-season analysis, or may be due to differences in leaf-temperature photosynthetic optima between sites. In agreement with our findings, Kolari et al. (2014) showed that the light reactions of photosynthesis (related to both SIF and GPP) were more sensitive to light but insensitive to air temperature compared to the enzymatic carbon reactions (related to GPP only).

Environmental controls on GPP and SIF_{red}

It is well established that light is a dominant control of both SIF and GPP, and we have shown that there are fundamental differences in the light responses of SIF_{red} and GPP throughout the year (Fig. 2). However, biological processes respond to the complex interactions between environmental controls (Reich et al., 2018; Wang et al., 2014). Therefore, we also asked when and how SIF_{red} and GPP differ in their sensitivity to other important environmental factors. By constructing ANNs with half-hourly data for each seasonal period, we investigated how their sub-daily responses to a suite of environmental drivers changed seasonally. Our results show the conditions under which we may not expect a uniform response of SIF and GPP.

The variability of GPP and SIF_{red} that is attributable to environmental drivers is shown in Fig. 4. There were notable differences in the responses of GPP and SIF_{red} to these drivers, and the patterns were different in each season. While PPFD was an important driver in spring, summer, and fall as expected, the amount of variability explained by PPFD alone changed in relation to the other drivers differently across seasons. The benchmark r^2 values (from an ANN with all drivers) showed that the combined candidate drivers explained 75%, 77%, 84% of the total variance in GPP in fall, summer, spring, respectively and 81%, 74%, 60% for those seasons in SIF_{red} (dashed lines in Fig. 4). The total explainable variability was highest for GPP but markedly lower for SIF_{red} in spring.

In the spring, no driver was considered as primary for GPP (PPFD, VWC, SWE, and SIF_{red} were tied after a Fisher r-z transformation), while there was a strong secondary influence of VWC and SWE when PPFD was used as the primary driver (Fig. 4). On the other hand, PPFD, T_{air} , and VPD tied for primary driver of SIF_{red} in spring, while there was no statistically best secondary driver. Therefore, water availability (VWC, SWE) in spring was an important secondary influence on GPP that was absent for SIF_{red}. This is in agreement with previous work at Niwot Ridge that has identified the timing of spring snowmelt as a primary control on early season GPP (Hu et al., 2010; Huxman et al., 2003; Monson et al., 2005, 2002; Albert et al., 2017). Additionally, the stronger role of T_{soil} over T_{air} was apparent for GPP but not SIF_{red}, suggesting SIF may not capture photosynthetic limitation by cold soils in spring (Ensminger et al., 2008).

As the forest emerged from snowmelt in summer, there was a transition in secondary control of GPP from soil moisture (spring) to T_{air} and VPD (summer). The important secondary role of VPD alongside T_{air} suggests that the light response of GPP was mediated by stomatal response to increased evaporative demand associated with high temperature, rather than photosynthetic temperature optima alone. These patterns were not evident in the SIF_{red} observations. Summer SIF_{red} was also controlled primarily by PPFD, with PRI appearing as a candidate for primary driver. During fall, PPFD and T_{soil} were important drivers of GPP, while fall SIF_{red} was controlled similarly as in summer: by PPFD, PRI, and temperature. Since PRI was as important a driver of SIF_{red} in summer and fall as PPFD, this suggests that 1) SIF_{red} may have been responding to changes in xanthophyll pigments, 2) the instrument footprints of SIF_{red} and PRI were better matched than the other drivers, or 3) both SIF_{red} and PRI are subject to the same illumination geometry effects. PPFD remained an important explanatory variable of SIF_{red} in winter, while there was no GPP in winter. Slight differences in the results of the ANN when GPP was partitioned using the daytime method (Laslopp et al., 2010) are discussed in the supplement (Fig. S5).

We also found that the addition of SIF_{red} as a secondary input to GPP alongside light did not provide notable model improvement, implying that SIF_{red} did not contribute much additional information beyond light by itself with respect to explaining GPP variation. On the other hand, the addition of PRI as a secondary input to PPFD resulted in a large performance improvement for predicting GPP in spring, performing even better than temperature. This difference in secondary driver importance between SIF_{red} and PRI was, however, limited to the spring season, perhaps because SIF_{red} and PRI co-varied to a greater degree in fall. This suggests that while SIF_{red} does not provide much additional information that is not already contained in light, PRI as a representation of the xanthophyll cycle or seasonal pigment pool shifts may provide important information regarding spring upregulation of photosynthesis (Wong et al., 2019; Wong and Gamon, 2015b).

Lastly, we found that precipitation had little to no importance for either GPP or SIF_{red} in any season, and therefore is not shown in Fig. 4 or 6. This was likely due to the decoupled timing of precipitation (mainly winter) and GPP (mainly summer)—reflected in the dominance of VWC and SWE during spring. It has been demonstrated that snowmelt is an important source of water throughout the growing season and buffers the forest from moisture variation during summer (Hu et al., 2010). It also is possible that response to warm-season precipitation lags after the rain event by more than twelve hours, in which case our ANN analysis would not detect the effects because it focused on simultaneous half hour time steps of climate variables, SIF_{red}, and GPP. Indeed, it has been shown that PRI exhibited a 2-3 day lag response to transpiration following monsoon precipitation pulse events in a montane conifer forest (J.C. Yang et al., 2020). This is not to say that precipitation is not an important environmental control (i.e. interannually), rather, the lack of importance likely reflects the temporal resolution (half-hourly) and duration (annual) of this study.

Because temperature affects not only enzyme kinetics, but also the physical phase of water, temperature and moisture effects appear intertwined in their seasonal influences on productivity, revealed both by our results as well as a previous ANN analysis performed at this site with daytime and nighttime daily averaged net ecosystem productivity (NEP) (Albert et al., 2017). To further assess the degree to which SIF_{red} responded to these ecohydrological controls on productivity, we compared the sensitivities of SIF_{red} and GPP to canopy conductance to water vapor (Fig. 5). Because snow sublimation represents significant flux of water vapor in this forest (Molotch et al., 2007) it can strongly impact canopy conductance calculations, so we limit our discussion of canopy conductance to the summer (snow-free) season only. We found that SIF_{red} was unrelated to canopy conductance ($R^2 = .04$), whereas GPP had a nonlinear relationship ($R^2 = .44$). In contrast with these results, Shan et al. (2019) found significant correlation between canopy conductance and SIF across time scales in a deciduous forest, cropland, and savanna. These differences demonstrate the importance of considering contrasting environmental conditions and plant functional types. Notable differences include that 1) seasonal changes in canopy conductance are controlled by variation in stomatal opening in evergreen forests, but not leaf area (as in deciduous forests), and that 2) our study forest was under water deficit in the year 2018 and therefore stomatal closure may have significantly altered the SIF-conductance relationship. These results combined with the findings from the ANN analysis strongly suggest that SIF is less sensitive to stomatal control than is GPP, in agreement with a new body of work (Cochavi et al., 2021; He et al., 2020b; Helm et al., 2020; Marrs et al., 2020). On a global scale Chen et al. (2021) found that the SIF-GPP relationship varied along a latitudinal gradient of moisture availability, further highlighting the need to understand how the SIF-GPP relationship is mediated by stomatal control.

Partial derivative sensitivities

We examined the normalized partial derivative (PaD) sensitivities of

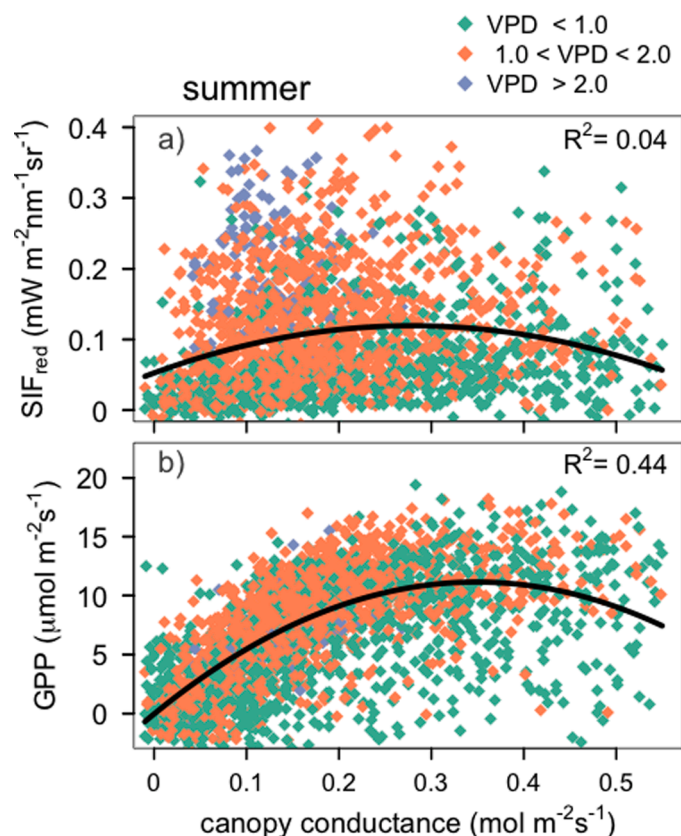


Fig. 5. The relationship between canopy conductance and a) SIF_{red} , and b) GPP in summer. Colored points represent data from the same VPD bins shown in Fig. S3, which divide the range of VPD for that season into equal thirds, with the lowest evaporative demand shown in green, mid-range in red, and highest in blue. Fit lines are 2nd order polynomials.

GPP to environmental conditions as well as to SIF_{red} and PRI (Fig. 6). Rather than ranking correlation coefficients as above, the PaD characterizes the change in the GPP functional response (magnitude and direction) with respect to changes in each input driver (Moffat et al., 2010). A large PaD sensitivity results from a large GPP response to a unit change in that driver, while the sign indicates if the response was increasing or decreasing. GPP had a strong sensitivity to VWC and SWE in spring. Compared to the positive T_{air} sensitivity in spring, in summer there was a negative sensitivity to VPD and partially negative sensitivity to T_{air} . These results reflect the spring to summer temperature pattern reversal in Fig. 3. In fall, GPP was highly responsive to warm, wet conditions. We found that the sensitivity of GPP to SIF_{red} was much weaker than to light, and was strongest in summer. These patterns suggest that SIF_{red} may be a sensitivity proxy for GPP in summer, but less so in spring or fall when GPP response to environmental conditions is highly dynamic and less sensitive to PPFD alone. Interestingly, while GPP sensitivity to SIF_{red} was quite weak in fall, GPP sensitivity to PRI was increased. This suggests that in fall GPP responds strongly to the combined effects of changes in the xanthophyll cycle and weather, and pigment-based indices such as PRI and CCI may be important for characterization of the fall transition period, in agreement with Kim et al. (2021). Further, a recent study at this site determined that the 530 nm spectral feature corresponding to changes in carotenoid content was important for tracking seasonality of LUE, and that SIF did not perform better than hyperspectral reflectance at tracking GPP phenology (Cheng et al., 2020).

Implications for the relationship between SIF and GPP

Our results show 1) there was an increase in SIF_{red} prior to the onset of spring GPP due to differences in their light responses, and that 2) SIF_{red} was less sensitive than GPP to seasonally dynamic temperature and soil and atmospheric moisture constraints. These results have important implications for the application of SIF in phenological studies. Monson et al. (2005) suggested that the winter to spring transition in this forest progresses from 1) PSII recovery initiated by warm T_{air} , 2) hydraulic system recovery, and 3) carbon reaction recovery. Under such a scenario, we would indeed expect to see an increase in SIF coincident with recovery of PSII prior to onset of GPP. Bowling et al. (2018) found that hydraulic system recovery was an important control for GPP recovery at Niwot Ridge, in agreement with the results of our ANN. In the present study SIF_{red} was mainly controlled by light and was less sensitive to temperature and moisture constraints in spring. These results suggest that SIF dynamics may be decoupled from hydraulic recovery, and support the idea that recovery of PSII occurs prior to both hydraulic and carbon reaction recovery. This contrasts with results from a boreal forest which found that increases in spring relative SIF_{red} corresponded with the timing of stem rehydration (Pierrat et al., 2021), which may reflect differences between mid and high latitude ecohydrology.

We highlight a couple of uncertainties that are important to consider when interpreting these results. First, the emission of fluorescence from PSII is a physiological process, however its measurement is affected by radiative transfer within the vegetation canopy. Because the wavelength region of SIF_{red} emission overlaps with the chlorophyll absorption spectrum, SIF_{red} is more sensitive to radiative transfer processes than is $SIF_{far-red}$ (Porcar-Castell et al., 2014), and variation in the $SIF_{red}/SIF_{far-red}$ ratio is caused by changes in chlorophyll content (Gitelson et al., 1998). However, Magney et al. (2019) used pigment data to show that chlorophyll concentration did not change across seasons at this site, so there was no discernable difference between SIF_{red} and $SIF_{far-red}$ for tracking GPP. They showed that SIF_{red} and $SIF_{far-red}$ scale linearly across the seasons on hourly-weekly timescales, and that $SIF_{far-red}$ is closely related to leaf level physiology at this forest (Magney et al., 2019). A complete understanding of how SIF_{red} measurements reflect physiological processes requires leaf-level observations, and future studies should examine the impact of reabsorption within the vegetation canopy carefully (Liu et al., 2020). A second source of uncertainty results from the unavoidable footprint mismatch between EC flux measurements and tower-based proximal remote sensing (Gamon, 2015). The difference in light response between GPP and SIF_{red} during the spring onset could reflect individual or species level variation in physiology, which may be exacerbated by the smaller radiometric footprint.

Global terrestrial biosphere models commonly predict spring onset of GPP in evergreen ecosystems as too early (Richardson et al., 2012; Anav et al., 2015; Parazoo et al., 2018), and this may be due to model oversensitivity to T_{air} . We found that that T_{air} influenced GPP primarily after the snowmelt period, supporting this idea. This oversensitivity may be exacerbated rather than ameliorated by the use of SIF to estimate GPP. Recent studies have pointed to the importance of accounting for soil moisture limitation in GPP products (Stocker et al., 2018) and highlighted the role of soil moisture in driving the interannual variability of global GPP (Li and Xiao, 2020). Thus, the elevated importance of spring soil moisture compared to temperature, and the discrepancy in the sensitivity of SIF_{red} to soil moisture, represent an important challenge for the use of SIF to predict spring onset of photosynthesis and moisture-related GPP constraints. Based on the results of our ANN ensemble analysis, we hypothesize that only after full hydraulic recovery and release from stomatal limitation in spring does APAR take on a dominant role in driving a linear (moderate light) or nonlinear (high light) SIF-GPP relationship.

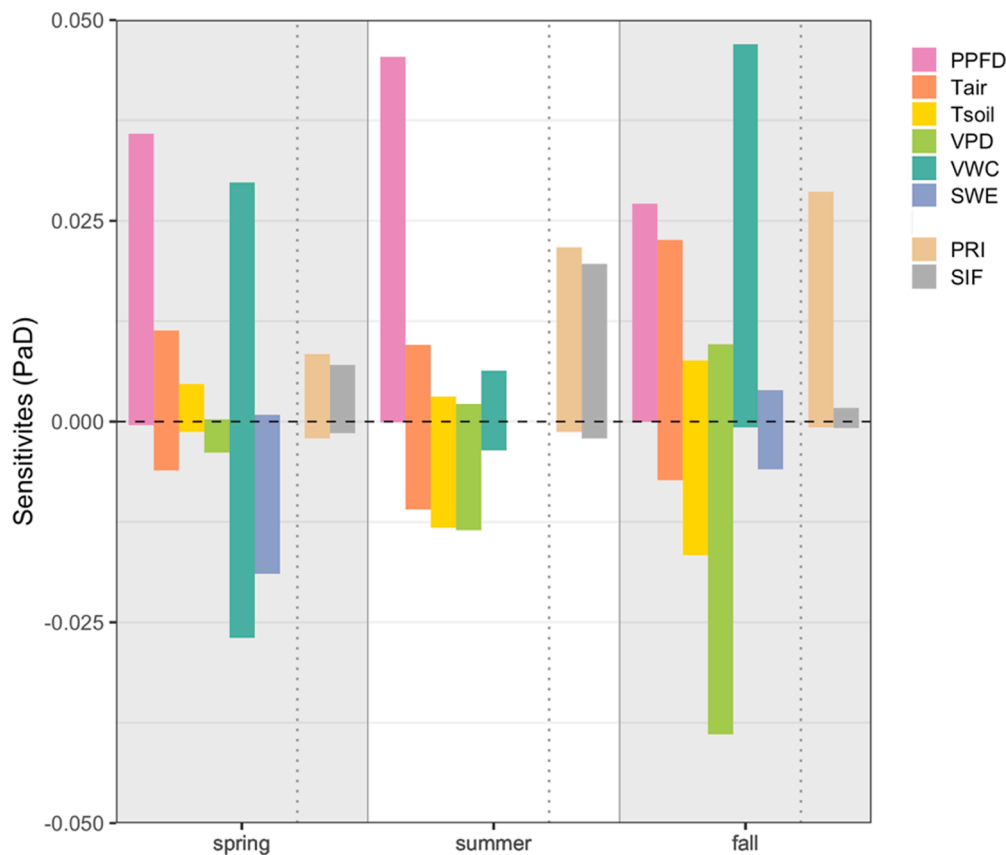


Fig. 6. The normalized positive and negative sensitivities (unitless) of the numerical partial derivatives (PaD) extracted from the GPP ANN. This is a profile of the magnitude and direction of the GPP response to changes of each driver.

Conclusion

In this study we used one year of continuous tower-based SIF_{red} and eddy covariance-derived GPP to examine when and how SIF_{red} and GPP differ in their responses to light. First, we asked when are there fundamental differences in the light responses of SIF_{red} and GPP? We found that SIF_{red} responded to light earlier in the year than the onset of GPP following winter dormancy. Second, we asked when and how do SIF_{red} and GPP differ in their response to environmental controls? An ANN ensemble analyses showed that the relative importance of environmental drivers for determining GPP and SIF_{red} changed seasonally, and GPP sensitivity to environmental constraints was more dynamic throughout the year than was the SIF_{red} sensitivity. Notably, we found that the variability in GPP explained by light changed in relation to temperature and moisture from spring to summer, while SIF_{red} was less affected by secondary drivers, particularly in spring. In agreement, we also found that SIF_{red} was not correlated with canopy conductance in summer. These results provide evidence that SIF emission is less sensitive to stomatal control of carbon and water fluxes than is GPP, and photosystems begin to activate in preparation for the growing season prior to when water becomes available for photosynthesis. These findings represent a challenge for the use of SIF to predict the start of the photosynthetic season in conifer forests.

Data Availability

Data from the PhotoSpec instrument are available from the data repository hosted at the California Institute of Technology: <https://data.caltech.edu/records/1231> (Magney et al., Canopy and needle scale fluorescence data from Niwot Ridge, Colorado 2017-2018 (Version 1.0). CaltechDATA. <https://doi.org/10.22002/d1.1231>). Eddy covariance

data from US-NR1 is available from Ameriflux at: <https://ameriflux.lbl.gov/>.

Supplement

Daytime Partitioned GPP: There were differences in the results of the ANNs based on the choice of NEE partitioning method. An equivalent version of Fig. 4 but with GPP determined from the daytime partitioning method (Lasslop et al., 2010) is shown in Fig. S5. The daytime partitioning method results in a modeling artifact at this site in which there are non-zero values of GPP during wintertime. This artifact had a large effect on the wintertime ANN results (Fig. S5), that should not be treated as ecologically meaningful. In agreement with ANNs trained on nighttime partitioned GPP, a combination of PPF and SWE had the best explanatory power in spring, and PPF was still the dominant driver in summer. In fall however, the daytime partitioning method data indicated a combination of PPF with VWC to be more important than with T_{soil} . The benchmark explanatory power of the network was markedly higher when trained on daytime partitioned GPP (>95% in spring and fall). Though both the nighttime and daytime partitioning methods produce a modeled GPP product, the daytime method uses light response curves to model GPP directly, potentially inflating its correlation to light. Therefore we emphasize that care should be taken to consider how GPP values are derived when performing any analysis, but in particular when training ANN with GPP.

Declaration of Competing Interest

The authors declare that they have no known competing financial interests or personal relationships that could have appeared to influence the work reported in this paper.

Acknowledgments

We would like to thank Trevor Keenan for providing Matlab code to run the ANN analysis on GitHub, as well as Sovan Lek for providing Matlab code to extract the PaD, Barry Logan for providing helpful discussion, Xueqian Wang for providing flux tower footprint data, and Blake Zimmerman for helping with partial derivative calculation. J. Yang gratefully acknowledges support from the Graduate Research Fellowship Program at the U.S. National Science Foundation. This work was supported by the NSF Macrosystems Biology and NEON-Enabled Science program at NSF (award 1926090). DB was supported by NASA Awards 80NSSC20K0010 and 80NSSC19M0130. US-NR1 was supported by DOE AmeriFlux Management Project subcontract number 7542010. The US-NR1 AmeriFlux site is supported by the U.S. DOE, Office of Science through the AmeriFlux Management Project (AMP) at Lawrence Berkeley National Laboratory under Award Number 7094866. The National Center for Atmospheric Research (NCAR) is sponsored by the NSF.

Supplementary materials

Supplementary material associated with this article can be found, in the online version, at doi:[10.1016/j.agrformet.2022.108904](https://doi.org/10.1016/j.agrformet.2022.108904).

References

- Abramowitz, G., 2005. Towards a benchmark for land surface models. *Geophysical Research Letters* 32. <https://doi.org/10.1029/2005GL024419>.
- Albert, L.P., Keenan, T.F., Burns, S.P., Huxman, T.E., Monson, R.K., 2017. Climate controls over ecosystem metabolism: insights from a fifteen-year inductive artificial neural network synthesis for a subalpine forest. *Oecologia* 184, 25–41. <https://doi.org/10.1007/s00442-017-3853-0>.
- Anav, A., Friedlingstein, P., Beer, C., Ciais, P., Harper, A., Jones, C., Murray-Tortarolo, G., Papale, D., Parazoo, N.C., Peylin, P., Piao, S., Sitch, S., Viovy, N., Wiltshire, A., Zhao, M., 2015. Spatiotemporal patterns of terrestrial gross primary production: A review. *Rev. Geophys.* 53, 2015RG0000483 <https://doi.org/10.1002/2015RG0000483>.
- Bauerle, W.L., Oren, R., Way, D.A., Qian, S.S., Stoy, P.C., Thornton, P.E., Bowden, J.D., Hoffman, F.M., Reynolds, R.F., 2012. Photoperiodic regulation of the seasonal pattern of photosynthetic capacity and the implications for carbon cycling. *Proceedings of the National Academy of Sciences of the United States of America* 109, 8612–8617.
- Beale, M.H., Hagan, M.T., Demuth, H.B., 2014. *Neural network toolbox™ user's guide. The MathWorks, Natick.*
- Beer, C., Reichstein, M., Tomelleri, E., Ciais, P., Jung, M., Carvalhais, N., Rodenbeck, C., Arain, M.A., Baldocchi, D., Bonan, G.B., Bondeau, A., Cescatti, A., Lasslop, G., Lindroth, A., Lomas, M., Luysaert, S., Margolis, H., Oleson, K.W., Rouspard, O., Veenendaal, E., Viovy, N., Williams, C., Woodward, F.I., Papale, D., 2010. Terrestrial Gross Carbon Dioxide Uptake: Global Distribution and Covariation with Climate. *Science* 329, 834–838. <https://doi.org/10.1126/science.1184984>.
- Biriukova, K., Celesti, M., Evdokimov, A., Pacheco-Labrador, J., Julitta, T., Migliavacca, M., Giardino, C., Miglietta, F., Colombo, R., Panigada, C., Rossini, M., 2020. Effects of varying solar-view geometry and canopy structure on solar-induced chlorophyll fluorescence and PRI. *International Journal of Applied Earth Observation and Geoinformation* 89, 102069. <https://doi.org/10.1016/j.jag.2020.102069>.
- Bishop, C.M., 1995. *Neural networks for pattern recognition.* Oxford University Press, Oxford.
- Björkman, O., Demmig-Adams, B., 1995. Regulation of Photosynthetic Light Energy Capture, Conversion, and Dissipation in Leaves of Higher Plants. In: Schulze, E.-D., Caldwell, M.M. (Eds.), *Ecophysiology of Photosynthesis*, Springer Study Edition. Springer, Berlin, Heidelberg, pp. 17–47. https://doi.org/10.1007/978-3-642-79354-7_2.
- Blanken, P.D., Black, T.A., Yang, P.C., Neumann, H.H., Nesic, Z., Staebler, R., Hartog, G., den, Novak, M.D., Lee, X., 1997. Energy balance and canopy conductance of a boreal aspen forest: Partitioning overstory and understory components. *Journal of Geophysical Research: Atmospheres* 102, 28915–28927. <https://doi.org/10.1029/97JD00193>.
- Bowling, D.R., Logan, B.A., Hufkens, K., Aubrecht, D.M., Richardson, A.D., Burns, S.P., Anderegg, W.R.L., Blanken, P.D., Eirikkson, D.P., 2018. Limitations to winter and spring photosynthesis of a Rocky Mountain subalpine forest. *Agricultural and Forest Meteorology* 252, 241–255. <https://doi.org/10.1016/j.agrformet.2018.01.025>.
- Burns, S.P., Blanken, P.D., Turnipseed, A.A., Hu, J., Monson, R.K., 2015. The influence of warm-season precipitation on the diel cycle of the surface energy balance and carbon dioxide at a Colorado subalpine forest site. *Biogeosciences* 12, 7349–7377. <https://doi.org/10.5194/bg-12-7349-2015>.
- Chang, Q., Xiao, X., Jiao, W., Wu, X., Doughty, R., Wang, J., Du, L., Zou, Z., Qin, Y., 2019. Assessing consistency of spring phenology of snow-covered forests as estimated by vegetation indices, gross primary production, and solar-induced chlorophyll fluorescence. *Agricultural and Forest Meteorology* 275, 305–316. <https://doi.org/10.1016/j.agrformet.2019.06.002>.
- Chen, A., Mao, J., Ricciuto, D., Xiao, J., Frankenberg, C., Li, X., Thornton, P.E., Gu, L., Knapp, A.K., 2021. Moisture availability mediates the relationship between terrestrial gross primary production and solar-induced chlorophyll fluorescence: Insights from global-scale variations. *Global Change Biology* 27, 1144–1156. <https://doi.org/10.1111/gcb.15373>.
- Cheng, R., Magney, T.S., Dutta, D., Bowling, D.R., Logan, B.A., Burns, S.P., Blanken, P.D., Grossmann, K., Lopez, S., Richardson, A.D., Stutz, J., Frankenberg, C., 2020. Decomposing reflectance spectra to track gross primary production in a subalpine evergreen forest. *Biogeosciences* 17, 4523–4544. <https://doi.org/10.5194/bg-17-4523-2020>.
- Cochavi, A., Amer, M., Stern, R., Tatarinov, F., Migliavacca, M., Yakir, D., 2021. Differential responses to two heatwave intensities in a Mediterranean citrus orchard are identified by combining measurements of fluorescence and carbonyl sulfide (COS) and CO₂ uptake. *New Phytologist* n/a. <https://doi.org/10.1111/nph.17247>.
- Dechant, B., Ryu, Y., Badgley, G., Zeng, Y., Berry, J.A., Zhang, Y., Goulas, Y., Li, Z., Zhang, Q., Kang, M., Li, J., Moya, I., 2020. Canopy structure explains the relationship between photosynthesis and sun-induced chlorophyll fluorescence in crops. *Remote Sensing of Environment* 241, 111733. <https://doi.org/10.1016/j.rse.2020.111733>.
- Demmig-Adams, B., Adams, W.W., 2006. Photoprotection in an ecological context: the remarkable complexity of thermal energy dissipation. *New Phytol* 172, 11–21. <https://doi.org/10.1111/j.1469-8137.2006.01835.x>.
- Demmig-Adams, B., Cohu, C.M., Muller, O., Adams, W.W., 2012. Modulation of photosynthetic energy conversion efficiency in nature: from seconds to seasons. *Photosynth. Res.* 113, 75–88. <https://doi.org/10.1007/s11120-012-9761-6>.
- Ensminger, I., Schmidt, L., Lloyd, J., 2008. Soil temperature and intermittent frost modulate the rate of recovery of photosynthesis in Scots pine under simulated spring conditions. *New Phytologist* 177, 428–442. <https://doi.org/10.1111/j.1469-8137.2007.02273.x>.
- Ensminger, I., Sveshnikov, D., Campbell, D.A., Funk, C., Jansson, S., Lloyd, J., Shibistova, O., Öquist, G., 2004. Intermittent low temperatures constrain spring recovery of photosynthesis in boreal Scots pine forests. *Global Change Biology* 10, 995–1008. <https://doi.org/10.1111/j.1365-2486.2004.00781.x>.
- Esteban, R., Barrutia, O., Artetxe, U., Fernández-Marín, B., Hernández, A., García-Plazaola, J.I., 2015. Internal and external factors affecting photosynthetic pigment composition in plants: a meta-analytical approach. *New Phytologist* 206, 268–280. <https://doi.org/10.1111/nph.13186>.
- Field, C.B., Randerson, J.T., Malmström, C.M., 1995. Global net primary production: Combining ecology and remote sensing. *Remote Sensing of Environment. Remote Sensing of Land Surface for Studies of Global Change* 51, 74–88. [https://doi.org/10.1016/0034-4257\(94\)00066-V](https://doi.org/10.1016/0034-4257(94)00066-V).
- Fisher, R.A., 1921. On the probable error of a coefficient of correlation deduced from a small sample. *Metron* 1, 3–32.
- Flexas, J., Escalona, J.M., Evain, S., Gulías, J., Moya, I., Osmond, C.B., Medrano, H., 2002. Steady-state chlorophyll fluorescence (Fs) measurements as a tool to follow variations of net CO₂ assimilation and stomatal conductance during water-stress in C3 plants. *Physiologia Plantarum* 114, 231–240. <https://doi.org/10.1034/j.1399-3054.2002.1140209.x>.
- Frankenberg, C., Butz, A., Toon, G.C., 2011a. Disentangling chlorophyll fluorescence from atmospheric scattering effects in O₂ A-band spectra of reflected sun-light. *Geophysical Research Letters* 38 (3). <https://doi.org/10.1029/2010GL045896>.
- Frankenberg, C., Fisher, J.B., Worden, J., Badgley, G., Saatchi, S.S., Lee, J.-E., Toon, G.C., Butz, A., Jung, M., Kuze, A., Yokota, T., 2011b. New global observations of the terrestrial carbon cycle from GOSAT: Patterns of plant fluorescence with gross primary productivity. *Geophys. Res. Lett.* 38, L17706. <https://doi.org/10.1029/2011GL048738>.
- Frankenberg, C., O'Dell, C., Berry, J., Guanter, L., Joiner, J., Köhler, P., Pollock, R., Taylor, T.E., 2014. Prospects for chlorophyll fluorescence remote sensing from the Orbiting Carbon Observatory-2. *Remote Sensing of Environment* 147, 1–12. <https://doi.org/10.1016/j.rse.2014.02.007>.
- Frechette, E., Wong, C.Y.S., Junker, L.V., Chang, C.Y.Y., Ensminger, I., 2015. Zeaxanthin-independent energy quenching and alternative electron sinks cause a decoupling of the relationship between the photochemical reflectance index (PRI) and photosynthesis in an evergreen conifer during spring. *J. Exp. Bot.* 66, 7309–7323. <https://doi.org/10.1093/jxb/erv427>.
- Gamon, J.A., 2015. Reviews and Syntheses: optical sampling of the flux tower footprint. *Biogeosciences* 12 (14), 4509–4523. <https://doi.org/10.5194/bg-12-4509-2015>.
- Gamon, J.A., Huemmrich, K.F., Wong, C.Y.S., Ensminger, I., Garrity, S., Hollinger, D.Y., Noormets, A., Peñauelas, J., 2016. A remotely sensed pigment index reveals photosynthetic phenology in evergreen conifers. *PNAS* 113, 13087–13092. <https://doi.org/10.1073/pnas.1606162113>.
- Gamon, J.A., Peñauelas, J., Field, C.B., 1992. A narrow-waveband spectral index that tracks diurnal changes in photosynthetic efficiency. *Remote Sensing of Environment* 41, 35–44. [https://doi.org/10.1016/0034-4257\(92\)90059-S](https://doi.org/10.1016/0034-4257(92)90059-S).
- Gamon John, A., Field Christopher, B., Goulden Michael, L., Griffin Kevin, L., Hartley Anne, E., Geeske, Joel, Josep, Penuelas, Riccardo, Valentini, 1995. Relationships Between NDVI, Canopy Structure, and Photosynthesis in Three Californian Vegetation Types. *Ecological Applications* 5, 28–41. <https://doi.org/10.2307/1942049>.
- Gevrey, M., Dimopoulos, I., Lek, S., 2003. Review and comparison of methods to study the contribution of variables in artificial neural network models. *Ecological Modelling*, Modelling the structure of aquatic communities: concepts, methods and problems 160, 249–264. [https://doi.org/10.1016/S0304-3800\(02\)00257-0](https://doi.org/10.1016/S0304-3800(02)00257-0).

- Gitelson, A.A., Buschmann, C., Lichtenthaler, H.K., 1998. Leaf chlorophyll fluorescence corrected for re-absorption by means of absorption and reflectance measurements. *Journal of plant physiology* 152 (2-3), 283–296. [https://doi.org/10.1016/S0176-1617\(98\)80143-0](https://doi.org/10.1016/S0176-1617(98)80143-0).
- Gitelson, A.A., Gamon, J.A., 2015. The need for a common basis for defining light-use efficiency: Implications for productivity estimation. *Remote Sens. Environ.* 156, 196–201. <https://doi.org/10.1016/j.rse.2014.09.017>.
- Goulden, M.L., Anderson, R.G., Bales, R.C., Kelly, A.E., Meadows, M., Winston, G.C., 2012. Evapotranspiration along an elevation gradient in California's Sierra Nevada. *Journal of Geophysical Research G: Biogeosciences* 117.
- Goward, S.N., Huemmrich, K.F., 1992. VEGETATION CANOPY PAR ABSORPTANCE AND THE NORMALIZED DIFFERENCE VEGETATION INDEX - AN ASSESSMENT USING THE SAIL MODEL. *Remote Sens. Environ.* 39, 119–140. [https://doi.org/10.1016/0034-4257\(92\)90131-3](https://doi.org/10.1016/0034-4257(92)90131-3).
- Grossmann, K., Frankenberg, C., Magney, T.S., Hurlock, S.C., Seibt, U., Stutz, J., 2018. PhotoSpec: A new instrument to measure spatially distributed red and far-red Solar-Induced Chlorophyll Fluorescence. *Remote Sensing of Environment* 216, 311–327. <https://doi.org/10.1016/j.rse.2018.07.002>.
- Gu, L., Han, J., Wood, J.D., Chang, C.Y.-Y., Sun, Y., 2019. Sun-induced Chl fluorescence and its importance for biophysical modeling of photosynthesis based on light reactions. *New Phytologist* 223, 1179–1191. <https://doi.org/10.1111/nph.15796>.
- Guanter, L., Frankenberg, C., Dudhia, A., Lewis, P.E., Gómez-Dans, J., Kuze, A., Suto, H., Grainger, R.G., 2012. Retrieval and global assessment of terrestrial chlorophyll fluorescence from GOSAT space measurements. *Remote Sensing of Environment* 121, 236–251. <https://doi.org/10.1016/j.rse.2012.02.006>.
- Guanter, L., Zhang, Y., Jung, M., Joiner, J., Voigt, M., Berry, J.A., Frankenberg, C., Huete, A.R., Zarco-Tejada, P., Lee, J.-E., Moran, M.S., Ponce-Campos, G., Beer, C., Camps-Valls, G., Buchmann, N., Gianelle, D., Klumpp, K., Cescatti, A., Baker, J.M., Griffis, T.J., 2014. Global and time-resolved monitoring of crop photosynthesis with chlorophyll fluorescence. *PNAS* 111, E1327–E1333. <https://doi.org/10.1073/pnas.1320008111>.
- He, L., Magney, T., Dutta, D., Yin, Y., Köhler, P., Grossmann, K., Stutz, J., Dold, C., Hatfield, J., Guan, K., Peng, B., Frankenberg, C., 2020a. From the Ground to Space: Using Solar-Induced Chlorophyll Fluorescence to Estimate Crop Productivity. *Geophysical Research Letters* 47, e2020GL087474. <https://doi.org/10.1029/2020GL087474>.
- He, L., Wood, J.D., Sun, Y., Magney, T., Dutta, D., Köhler, P., Zhang, Y., Yin, Y., Frankenberg, C., 2020b. Tracking Seasonal and Interannual Variability in Photosynthetic Downregulation in Response to Water Stress at a Temperate Deciduous Forest. *Journal of Geophysical Research: Biogeosciences* 125, e2018JG005002. <https://doi.org/10.1029/2018JG005002>.
- Helm, L.T., Shi, H., Lerdau, M.T., Yang, X., 2020. Solar-induced chlorophyll fluorescence and short-term photosynthetic response to drought. *Ecological Applications* n/a. <https://doi.org/10.1002/eap.2101>.
- Hall, F.G., Hilker, T., Coops, N.C., Lyapustin, A., Huemmrich, K.F., Middleton, E., Margolis, H., Drolet, G., Black, T.A., 2008. Multi-angle remote sensing of forest light use efficiency by observing PRI variation with canopy shadow fraction. *Remote Sensing of Environment* 112 (7), 3201–3211. <https://doi.org/10.1016/j.rse.2008.03.015>.
- Hilker, T., Coops, N.C., Wulder, M.A., Black, T.A., Guy, R.D., 2008. The use of remote sensing in light use efficiency based models of gross primary production: A review of current status and future requirements. *Sci. Total Environ.* 404, 411–423. <https://doi.org/10.1016/j.scitotenv.2007.11.007>.
- Hu, J., Moore, D.J.P., Burns, S.P., Monson, R.K., 2010. Longer growing seasons lead to less carbon sequestration by a subalpine forest. *Global Change Biology* 16, 771–783. <https://doi.org/10.1111/j.1365-2486.2009.01967.x>.
- Huxman, T.E., Turnipseed, A.A., Sparks, J.P., Harley, P.C., Monson, R.K., 2003. Temperature as a control over ecosystem CO₂ fluxes in a high-elevation, subalpine forest. *Oecologia* 134, 537–546. <https://doi.org/10.1007/s00442-002-1131-1>.
- Jeong, S.J., Schimel, D., Frankenberg, C., Drewry, D.T., Fisher, J.B., Verma, M., Joiner, J., 2017. Application of satellite solar-induced chlorophyll fluorescence to understanding large-scale variations in vegetation phenology and function over northern high latitude forests. *Remote Sensing of Environment* 190, 178–187. <https://doi.org/10.1016/j.rse.2016.11.021>.
- Joiner, J., Yoshida, Y., Vasilkov, A.P., Yoshida, Y., Corp, L.A., Middleton, E.M., 2011. First observations of global and seasonal terrestrial chlorophyll fluorescence from space. *Biogeosciences* 8, 637–651. <https://doi.org/10.5194/bg-8-637-2011>.
- Keenan, T.F., Davidson, E., Moffat, A.M., Munger, W., Richardson, A.D., 2012. Using model-data fusion to interpret past trends, and quantify uncertainties in future projections, of terrestrial ecosystem carbon cycling. *Global Change Biology* 18, 2555–2569.
- Kim, J., Ryu, Y., Dechant, B., Lee, H., Kim, H.S., Kornfeld, A., Berry, J.A., 2021. Solar-induced chlorophyll fluorescence is non-linearly related to canopy photosynthesis in a temperate evergreen needleleaf forest during the fall transition. *Remote Sensing of Environment* 258, 112362. <https://doi.org/10.1016/j.rse.2021.112362>.
- Knowles, J.F., Burns, S.P., Blanken, P.D., Monson, R.K., 2015. Fluxes of energy, water, and carbon dioxide from mountain ecosystems at Niwot Ridge, Colorado. *Plant Ecology & Diversity* 8 (5-6), 663–676. <https://doi.org/10.1080/17550874.2014.904950>.
- Knowles, J.F., Scott, R.L., Biederman, J.A., Blanken, P.D., Burns, S.P., Dore, S., Kolb, T.E., Litvak, M.E., Barron-Gafford, G.A., 2020. Montane forest productivity across a semi-arid climatic gradient. *Global Change Biology* 26, 6945–6958. <https://doi.org/10.1111/gcb.15335>.
- Kolari, P., Chan, T., Porcar-Castell, A., Bäck, J., Nikinmaa, E., Juurola, E., 2014. Field and controlled environment measurements show strong seasonal acclimation in photosynthesis and respiration potential in boreal Scots pine. *Front. Plant Sci* 5, 717. <https://doi.org/10.3389/fpls.2014.00717>.
- Lasslop, G., Reichstein, M., Papale, D., Richardson, A., Arneth, A., Barr, A., Stoy, P., Wohlfahrt, G., 2010. Separation of net ecosystem exchange into assimilation and respiration using a light response curve approach: critical issues and global evaluation. *Global Change Biology* 16, 187–208.
- Lek, S., Guégan, J.-F., 1999. Artificial neural networks as a tool in ecological modelling, an introduction. *Ecological Modelling* 120, 65–73.
- Li, X., Xiao, J., 2020. Global climatic controls on interannual variability of ecosystem productivity: Similarities and differences inferred from solar-induced chlorophyll fluorescence and enhanced vegetation index. *Agricultural and Forest Meteorology*, 108018. <https://doi.org/10.1016/j.agrformet.2020.108018>.
- Li, X., Xiao, J., He, B., Arain, M.A., Beringer, J., Desai, A.R., Emmel, C., Hollinger, D.Y., Krasnova, A., Mammarella, I., Noe, S.M., Ortiz, P.S., Rey-Sanchez, A.C., Rocha, A.V., Varlagin, A., 2018. Solar-induced chlorophyll fluorescence is strongly correlated with terrestrial photosynthesis for a wide variety of biomes: First global analysis based on OCO-2 and flux tower observations. *Global Change Biology* 24, 3990–4008. <https://doi.org/10.1111/gcb.14297>.
- Liu, X., Liu, L., Hu, J., Guo, J., Du, S., 2020. Improving the potential of red SIF for estimating GPP by downscaling from the canopy level to the photosystem level. *Agricultural and Forest Meteorology* 281, 107846.
- Magney, T.S., Barnes, M.L., Yang, X., 2020. On the Covariation of Chlorophyll Fluorescence and Photosynthesis Across Scales. *Geophysical Research Letters* 47, e2020GL091098. <https://doi.org/10.1029/2020GL091098>.
- Magney, T.S., Bowling, D.R., Logan, B.A., Grossmann, K., Stutz, J., Blanken, P.D., Burns, S.P., Cheng, R., Garcia, M.A., Köhler, P., Lopez, S., Parazoo, N.C., Raczka, B., Schimel, D., Frankenberg, C., 2019. Mechanistic evidence for tracking the seasonality of photosynthesis with solar-induced fluorescence. *PNAS* 116, 11640–11645. <https://doi.org/10.1073/pnas.1900278116>.
- Marrs, J.K., Reblin, J.S., Logan, B.A., Allen, D.W., Reinmann, A.B., Bombard, D.M., Tabachnik, D., Hutrya, L.R., 2020. Solar-Induced Fluorescence Does Not Track Photosynthetic Carbon Assimilation Following Induced Stomatal Closure. *Geophysical Research Letters* 47, e2020GL087956. <https://doi.org/10.1029/2020GL087956>.
- Maurer, G.E., Bowling, D.R., 2014. Seasonal snowpack characteristics influence soil temperature and water content at multiple scales in interior western U.S. mountain ecosystems. *Water Resour. Res.* 50, 5216–5234. <https://doi.org/10.1002/2013WR014452>.
- Maxwell, K., Johnson, G.N., 2000. Chlorophyll fluorescence - a practical guide. *J. Exp. Bot.* 51, 659–668. <https://doi.org/10.1093/jexbot/51.345.659>.
- Miao, G., Guan, K., Yang, X., Bernacchi, C.J., Berry, J.A., DeLucia, E.H., Wu, J., Moore, C. E., Meacham, K., Cai, Y., Peng, B., Kimm, H., Masters, M.D., 2018. Sun-Induced Chlorophyll Fluorescence, Photosynthesis, and Light Use Efficiency of a Soybean Field from Seasonally Continuous Measurements. *Journal of Geophysical Research: Biogeosciences* 123, 610–623. <https://doi.org/10.1002/2017JG004180>.
- Moffat, A.M., 2012. A new methodology to interpret high resolution measurements of net carbon fluxes between terrestrial ecosystems and the atmosphere 124.
- Moffat, A.M., Beckstein, C., Churkina, G., Mund, M., Heimann, M., 2010. Characterization of ecosystem responses to climatic controls using artificial neural networks. *Global Change Biology* 16, 2737–2749. <https://doi.org/10.1111/j.1365-2486.2010.02171.x>.
- Mohammed, G.H., Colombo, R., Middleton, E.M., Rascher, U., van der Tol, C., Nedbal, L., Goulas, Y., Pérez-Priego, O., Damm, A., Meroni, M., Joiner, J., Cogliati, S., Verhoef, W., Malenovsky, Z., Gastellu-Etchegorry, J.-P., Miller, J.R., Guanter, L., Moreno, J., Moya, I., Berry, J.A., Frankenberg, C., Zarco-Tejada, P.J., 2019. Remote sensing of solar-induced chlorophyll fluorescence (SIF) in vegetation: 50 years of progress. *Remote Sensing of Environment* 231, 111177. <https://doi.org/10.1016/j.rse.2019.04.030>.
- Molotch, N.P., Blanken, P.D., Williams, M.W., Turnipseed, A.A., Monson, R.K., Margulis, S.A., 2007. Estimating sublimation of intercepted and sub-canopy snow using eddy covariance systems. *Hydrol. Process.* 21, 1567–1575. <https://doi.org/10.1002/hyp.6719>.
- Monson, R.K., Sparks, J.P., Rosenstiel, T.N., Scott-Denton, L.E., Huxman, T.E., Harley, P.C., Turnipseed, A.A., Burns, S.P., Backlund, B., Hu, J., 2005. Climatic influences on net ecosystem CO₂ exchange during the transition from wintertime carbon source to springtime carbon sink in a high-elevation, subalpine forest. *Oecologia* 146, 130–147.
- Monson, R.K., Turnipseed, A.A., Sparks, J.P., Harley, P.C., Scott-Denton, L.E., Sparks, K., Huxman, T.E., 2002. Carbon sequestration in a high-elevation, subalpine forest. *Global Change Biol. Global Change Biol* 8, 459–478.
- Monteith, J.L., 1977. Climate and the efficiency of crop production in Britain. *Philosophical Transaction of the Royal Society of London B281*, 277–294.
- Monteith, J.L., 1972. Solar Radiation and Productivity in Tropical Ecosystems. *Journal of Applied Ecology* 9, 747–766. <https://doi.org/10.2307/2401901>.
- Myneni, R.B., Williams, D.L., 1994. ON THE RELATIONSHIP BETWEEN FAPAR AND NDVI. *Remote Sens. Environ.* 49, 200–211. [https://doi.org/10.1016/0034-4257\(94\)90016-7](https://doi.org/10.1016/0034-4257(94)90016-7).
- Olden, J.D., Lawler, J.J., Poff, N.L., 2008. Machine learning methods without tears: a primer for ecologists. *The Quarterly Review of Biology* 83, 171–193. <https://doi.org/10.1086/587826>.
- Ottander, C., Campbell, D., Öquist, G., 1995. Seasonal changes in photosystem II organisation and pigment composition in *Pinus sylvestris*. *Planta* 197, 176–183. <https://doi.org/10.1007/BF00239954>.
- Papale, D., Valentini, R., 2003. A new assessment of European forests carbon exchanges by eddy fluxes and artificial neural network spatialization. *Global Change Biology* 9, 525–535.

- Parazoo, N.C., Arneht, A., Pugh, T.A.M., Smith, B., Steiner, N., Luus, K., Commane, R., Benmergui, J., Stofferahn, E., Liu, J., Rödenbeck, C., Kawa, R., Euskirchen, E., Zona, D., Arndt, K., Oechel, W., Miller, C., 2018. Spring photosynthetic onset and net CO₂ uptake in Alaska triggered by landscape thawing. *Global Change Biology* 24, 3416–3435. <https://doi.org/10.1111/gcb.14283>.
- Parazoo, N.C., Bowman, K., Fisher, J.B., Frankenberg, C., Jones, D.B.A., Gescatti, A., Pérez-Priego, Ó., Wohlfahrt, G., Montagnani, L., 2014. Terrestrial gross primary production inferred from satellite fluorescence and vegetation models. *Glob Change Biol* 20, 3103–3121. <https://doi.org/10.1111/gcb.12652>.
- Piao, S.L., Sitch, S., Ciais, P., Friedlingstein, P., Peylin, P., Wang, X.H., Ahlstrom, A., Anav, A., Canadell, J.G., Cong, N., Huntingford, C., Jung, M., Levis, S., Levy, P.E., Li, J.S., Lin, X., Lomas, M.R., Lu, M., Luo, Y.Q., Ma, Y.C., Myneni, R.B., Poulter, B., Sun, Z.Z., Wang, T., Viovy, N., Zaehle, S., Zeng, N., 2013. Evaluation of terrestrial carbon cycle models for their response to climate variability and to CO₂ trends. *Global Change Biology* 19, 2117–2132. <https://doi.org/10.1111/gcb.12187>.
- Pierrat, Z., Nehemy, M.F., Roy, A., Magney, T., Parazoo, N.C., Laroque, C., Pappas, C., Sonnentag, O., Grossmann, K., Bowling, D.R., Seibt, U., Ramirez, A., Johnson, B., Helgason, W., Barr, A., Stutz, J., 2021. Tower-Based Remote Sensing Reveals Mechanisms Behind a Two-phased Spring Transition in a Mixed-Species Boreal Forest. *Journal of Geophysical Research: Biogeosciences* 126, e2020JG006191. <https://doi.org/10.1029/2020JG006191>.
- Plascyk, J.A., Gabriel, F.C., 1975. The Fraunhofer Line Discriminator MKII—An Airborne Instrument for Precise and Standardized Ecological Luminescence Measurement. *IEEE Transactions on Instrumentation and Measurement* 24, 306–313. <https://doi.org/10.1109/TIM.1975.4314448>.
- Polgar, C.A., Primack, R.B., 2011. Leaf-out phenology of temperate woody plants: from trees to ecosystems. *New Phytologist* 191, 926–941. <https://doi.org/10.1111/j.1469-8137.2011.03803.x>.
- Porcar-Castell, A., 2011. A high-resolution portrait of the annual dynamics of photochemical and non-photochemical quenching in needles of *Pinus sylvestris*. *Physiol. Plant* 143, 139–153. <https://doi.org/10.1111/j.1399-3054.2011.01488.x>.
- Porcar-Castell, A., Garcia-Plazaola, J.I., Nichol, C.J., Kolari, P., Olascoaga, B., Kuusinen, N., Fernandez-Marin, B., Pulkkinen, M., Juurola, E., Nikinmaa, E., 2012. Physiology of the seasonal relationship between the photochemical reflectance index and photosynthetic light use efficiency. *Oecologia* 170, 313–323. <https://doi.org/10.1007/s00442-012-2317-9>.
- Porcar-Castell, A., Tyystjarvi, E., Atherton, J., van der Tol, C., Flexas, J., Pfundel, E.E., Moreno, J., Frankenberg, C., Berry, J.A., 2014. Linking chlorophyll a fluorescence to photosynthesis for remote sensing applications: mechanisms and challenges. *J. Exp. Bot* 65, 4065–4095. <https://doi.org/10.1093/jxb/eru191>.
- Reich, P.B., Sendall, K.M., Stefanski, A., Rich, R.L., Hobbie, S.E., Montgomery, R.A., 2018. Effects of climate warming on photosynthesis in boreal tree species depend on soil moisture. *Nature* 562, 263. <https://doi.org/10.1038/s41586-018-0582-4>.
- Reichstein, M., Falge, E., Baldocchi, D., Papale, D., Aubinet, M., Berbigier, P., Bernhofer, C., Buchmann, N., Gilmanov, T., Granier, A., Grunwald, T., Havrankova, K., Ilvesniemi, H., Janous, D., Knohl, A., Laurila, T., Lohila, A., Loustau, D., Matteucci, G., Meyers, T., Miglietta, F., Ourcival, J.M., Pumpanen, J., Rambal, S., Rotenberg, E., Sanz, M., Tenhunen, J., Seufert, G., Vaccari, F., Vesala, T., Yakir, D., Valentini, R., 2005. On the separation of net ecosystem exchange into assimilation and ecosystem respiration: review and improved algorithm. *Global Change Biology* 11, 1424–1439.
- Richardson, A.D., 2019. Tracking seasonal rhythms of plants in diverse ecosystems with digital camera imagery. *New Phytologist* 222, 1742–1750. <https://doi.org/10.1111/nph.15591>.
- Richardson, A.D., Anderson, R.S., Arain, M.A., Barr, A.G., Bohrer, G., Chen, G., Chen, J. M., Ciais, P., Davis, K.J., Desai, A.R., Dietze, M.C., Dragoni, D., Garrity, S.R., Gough, C.M., Grant, R., Hollinger, D.Y., Margolis, H.A., McCaughey, H., Migliavacca, M., Monson, R.K., Munger, J.W., Poulter, B., Raczka, B.M., Ricciuto, D. M., Sahoo, A.K., Schaefer, K., Tian, H., Vargas, R., Verbeeck, H., Xiao, J., Xue, Y., 2012. Terrestrial biosphere models need better representation of vegetation phenology: results from the North American Carbon Program Site Synthesis. *Glob Change Biol* 18, 566–584. <https://doi.org/10.1111/j.1365-2486.2011.02562.x>.
- Richardson, A.D., Bailey, A.S., Denny, E.G., Martin, C.W., O'keefe, J., 2006. Phenology of a northern hardwood forest canopy. *Global Change Biology* 12, 1174–1188. <https://doi.org/10.1111/j.1365-2486.2006.01164.x>.
- Rojas, R., 1996. *Neural Networks – A Systematic Introduction*. Springer, Berlin, Heidelberg.
- Running, S.W., Nemani, R.R., Heinsch, F.A., Zhao, M.S., Reeves, M., Hashimoto, H., 2004. A continuous satellite-derived measure of global terrestrial primary production. *Bioscience* 54, 547–560. [https://doi.org/10.1641/0006-3568\(2004\)054\[0547:acsmog\]2.0.co;2](https://doi.org/10.1641/0006-3568(2004)054[0547:acsmog]2.0.co;2).
- Ryu, Y., Berry, J.A., Baldocchi, D.D., 2019. What is global photosynthesis? History, uncertainties and opportunities. *Remote Sensing of Environment* 223, 95–114. <https://doi.org/10.1016/j.rse.2019.01.016>.
- Sage, R.F., Kubien, D.S., 2007. The temperature response of C₃ and C₄ photosynthesis. *Plant, Cell & Environment* 30, 1086–1106. <https://doi.org/10.1111/j.1365-3040.2007.01682.x>.
- Sellers, P.J., 1985. CANOPY REFLECTANCE, PHOTOSYNTHESIS AND TRANSPIRATION. *Int. J. Remote Sens.* 6, 1335–1372. <https://doi.org/10.1080/01431168508948283>.
- Sevanto, S., Suni, T., Pumpanen, J., Gr nholm, T., Kolari, P., Nikinmaa, E., Hari, P., Vesala, T., 2006. Wintertime photosynthesis and water uptake in a boreal forest. *Tree Physiology* 26, 749–757.
- Smith, W.K., Biederman, J.A., Scott, R.L., Moore, D.J.P., He, M., Kimball, J.S., Yan, D., Hudson, A., Barnes, M.L., MacBean, N., Fox, A.M., Litvak, M.E., 2018. Chlorophyll Fluorescence Better Captures Seasonal and Interannual Gross Primary Productivity Dynamics Across Dryland Ecosystems of Southwestern North America. *Geophysical Research Letters* 45, 748–757. <https://doi.org/10.1002/2017GL075922>.
- Smith, W.K., Dannenberg, M.P., Yan, D., Herrmann, S., Barnes, M.L., Barron-Gafford, G. A., Biederman, J.A., Ferrenberg, S., Fox, A.M., Hudson, A., Knowles, J.F., MacBean, N., Moore, D.J.P., Nagler, P.L., Reed, S.C., Rutherford, W.A., Scott, R.L., Wang, X., Yang, J., 2019. Remote sensing of dryland ecosystem structure and function: Progress, challenges, and opportunities. *Remote Sensing of Environment* 233, 111401. <https://doi.org/10.1016/j.rse.2019.111401>.
- Smith, W.K., Reed, S.C., Cleveland, C.C., Ballantyne, A.P., Anderegg, W.R.L., Wieder, W. R., Liu, Y.Y., Running, S.W., 2016. Large divergence of satellite and Earth system model estimates of global terrestrial CO₂ fertilization. *Nature Climate Change* 6, 306–310. <https://doi.org/10.1038/nclimate2879>.
- Springer, K.R., Wang, R., Gamon, J.A., 2017. Parallel Seasonal Patterns of Photosynthesis, Fluorescence, and Reflectance Indices in Boreal Trees. *Remote Sens* 9, 18. <https://doi.org/10.3390/rs9070691>.
- Stocker, B.D., Zscheischler, J., Keenan, T.F., Prentice, I.C., Peñuelas, J., Seneviratne, S.I., 2018. Quantifying soil moisture impacts on light use efficiency across biomes. *New Phytologist* 218, 1430–1449. <https://doi.org/10.1111/nph.15123>.
- Sun, Y., Frankenberg, C., Jung, M., Joiner, J., Guanter, L., Köhler, P., Magney, T., 2018. Overview of Solar-Induced chlorophyll Fluorescence (SIF) from the Orbiting Carbon Observatory-2: Retrieval, cross-mission comparison, and global monitoring for GPP. *Remote Sensing of Environment*. <https://doi.org/10.1016/j.rse.2018.02.016>.
- Sun, Y., Frankenberg, C., Wood, J.D., Schimel, D.S., Jung, M., Guanter, L., Drewry, D.T., Verma, M., Porcar-Castell, A., Griffis, T.J., Gu, L., Magney, T.S., Köhler, P., Evans, B., Yuen, K., 2017.OCO-2 advances photosynthesis observation from space via solar-induced chlorophyll fluorescence. *Science* 358, eaam5747. <https://doi.org/10.1126/science.aam5747>.
- Tucker, C.J., 1979. Red and photographic infrared linear combinations for monitoring vegetation. *Remote Sensing of Environment* 8, 127–150. [https://doi.org/10.1016/0034-4257\(79\)90013-0](https://doi.org/10.1016/0034-4257(79)90013-0).
- Turner, D.P., Ritts, W.D., Cohen, W.B., Maeirsperger, T.K., Gower, S.T., Kirschbaum, A. A., Running, S.W., Zhao, M.S., Wofsy, S.C., Dunn, A.L., Law, B.E., Campbell, J.L., Oechel, W.C., Kwon, H.J., Meyers, T.P., Small, E.E., Kurc, S.A., Gamon, J.A., 2005. Site-level evaluation of satellite-based global terrestrial gross primary production and net primary production monitoring. *Global Change Biology* 11, 666–684.
- van der Tol, C., Berry, J.A., Campbell, P.K.E., Rascher, U., 2014. Models of fluorescence and photosynthesis for interpreting measurements of solar-induced chlorophyll fluorescence. *J. Geophys. Res.-Biogeosci.* 119, 2312–2327. <https://doi.org/10.1002/2014jg002713>.
- Verhoeven, A., 2014. Sustained energy dissipation in winter evergreens. *New Phytologist* 201, 57–65. <https://doi.org/10.1111/nph.12466>.
- Verma, S.B., 1989. *Aerodynamic resistances to transfers of heat, mass and momentum*. IAHS-AISH publication, pp. 13–20.
- Verrelst, J., van der Tol, C., Magnani, F., Sabater, N., Rivera, J.P., Mohammed, G., Moreno, J., 2016. Evaluating the predictive power of sun-induced chlorophyll fluorescence to estimate net photosynthesis of vegetation canopies: A SCOPE modeling study. *Remote Sens. Environ.* 176, 139–151. <https://doi.org/10.1016/j.rse.2016.01.018>.
- Viña, A., Gitelson, A.A., 2005. New developments in the remote estimation of the fraction of absorbed photosynthetically active radiation in crops. *Geophysical Research Letters* 32. <https://doi.org/10.1029/2005GL023647>.
- Walther, S., Voigt, M., Thum, T., Gonsamo, A., Zhang, Y.G., Kohler, P., Jung, M., Varlagin, A., Guanter, L., 2016. Satellite chlorophyll fluorescence measurements reveal large-scale decoupling of photosynthesis and greenness dynamics in boreal evergreen forests. *Glob. Change Biol.* 22, 2979–2996. <https://doi.org/10.1111/gcb.13200>.
- Wang, X., Piao, S., Ciais, P., Friedlingstein, P., Myneni, R.B., Cox, P., Heimann, M., Miller, J., Peng, S., Wang, T., Yang, H., Chen, A., 2014. A two-fold increase of carbon cycle sensitivity to tropical temperature variations. *Nature advance online publication*. <https://doi.org/10.1038/nature12915>.
- Way, D.A., Stinziano, J.R., Berghoff, H., Oren, R., 2017. How well do growing season dynamics of photosynthetic capacity correlate with leaf biochemistry and climate fluctuations? *Tree Physiol* 37, 879–888. <https://doi.org/10.1093/treephys/tpx086>.
- Wieneke, S., Burkart, A., Cendrero-Mateo, M.P., Julitta, T., Rossini, M., Schickling, A., Schmidt, M., Rascher, U., 2018. Linking photosynthesis and sun-induced fluorescence at sub-daily to seasonal scales. *Remote sensing of environment* 219, 247–258. <https://doi.org/10.1016/j.rse.2018.10.019>.
- Wohlfahrt, G., Gerdel, K., Migliavacca, M., Rotenberg, E., Tatarinov, F., Müller, J., Hammerle, A., Julitta, T., Spielmann, F.M., Yakir, D., 2018. Sun-induced fluorescence and gross primary productivity during a heat wave. *Scientific reports* 8 (1), 1–9. <https://doi.org/10.1038/s41598-018-32602-z>.
- Wong, C.Y.S., D'Odorico, P., Arain, M.A., Ensminger, I., 2020. Tracking the phenology of photosynthesis using carotenoid-sensitive and near-infrared reflectance vegetation indices in a temperate evergreen and mixed deciduous forest. *New Phytologist*. <https://doi.org/10.1111/nph.16479>.
- Wong, C.Y.S., D'Odorico, P., Bhatena, Y., Arain, M.A., Ensminger, I., 2019. Carotenoid based vegetation indices for accurate monitoring of the phenology of photosynthesis at the leaf-scale in deciduous and evergreen trees. *Remote Sensing of Environment* 233, 111407. <https://doi.org/10.1016/j.rse.2019.111407>.
- Wong, C.Y.S., Gamon, J.A., 2015a. Three causes of variation in the photochemical reflectance index (PRI) in evergreen conifers. *New Phytol* 206, 187–195. <https://doi.org/10.1111/nph.13159>.
- Wong, C.Y.S., Gamon, J.A., 2015b. The photochemical reflectance index provides an optical indicator of spring photosynthetic activation in evergreen conifers. *New Phytol* 206, 196–208. <https://doi.org/10.1111/nph.13251>.

- Wood, J.D., Griffis, T.J., Baker, J.M., Frankenberg, C., Verma, M., Yuen, K., 2017. Multiscale analyses of solar-induced fluorescence and gross primary production. *Geophys. Res. Lett.* 44, 533–541. <https://doi.org/10.1002/2016gl070775>.
- Wu, C., Gonsamo, A., Chen, J.M., Kurz, W.A., Price, D.T., Lafleur, P.M., Jassal, R.S., Dragoni, D., Bohrer, G., Gough, C.M., Verma, S.B., Suyker, A.E., Munger, J.W., 2012. Interannual and spatial impacts of phenological transitions, growing season length, and spring and autumn temperatures on carbon sequestration: A North America flux data synthesis. *Global and Planetary Change* 92–93, 179–190. <https://doi.org/10.1016/j.gloplacha.2012.05.021>.
- Wu, G., Guan, K., Jiang, C., Peng, B., Kimm, H., Chen, M., Yang, X., Wang, S., Suyker, A. E., Bernacchi, C.J., Moore, C.E., Zeng, Y., Berry, J.A., Cendrero-Mateo, M.P., 2020. Radiance-based NIRv as a proxy for GPP of corn and soybean. *Environ. Res. Lett.* 15, 034009 <https://doi.org/10.1088/1748-9326/ab65cc>.
- Wutzler, T., Lucas-Moffat, A., Migliavacca, M., Knauer, J., Sickel, K., Šigut, L., Menzer, O., Reichstein, M., 2018. Basic and extensible post-processing of eddy covariance flux data with REddyProc. *Biogeosciences* 15, 5015–5030. <https://doi.org/10.5194/bg-15-5015-2018>.
- Yang, J.C., Magney, T.S., Yan, D., Knowles, J.F., Smith, W.K., Scott, R.L., Barron-Gafford, G.A., 2020. The Photochemical Reflectance Index (PRI) Captures the Ecohydrologic Sensitivity of a Semiarid Mixed Conifer Forest. *Journal of Geophysical Research: Biogeosciences* 125, e2019JG005624. <https://doi.org/10.1029/2019JG005624>.
- Yang, K., Ryu, Y., Dechant, B., Berry, J.A., Hwang, Y., Jiang, C., Kang, M., Kim, J., Kimm, H., Kornfeld, A., Yang, X., 2018. Sun-induced chlorophyll fluorescence is more strongly related to absorbed light than to photosynthesis at half-hourly resolution in a rice paddy. *Remote Sensing of Environment* 216, 658–673. <https://doi.org/10.1016/j.rse.2018.07.008>.
- Yang, P., van der Tol, C., 2018. Linking canopy scattering of far-red sun-induced chlorophyll fluorescence with reflectance. *Remote Sensing of Environment* 209, 456–467. <https://doi.org/10.1016/j.rse.2018.02.029>.
- Yang, P., Van der Tol, C., Campbell, P.K.E., Middleton, E.M., 2020. Unravelling the physical and physiological basis for the solar-induced chlorophyll fluorescence and photosynthesis relationship. *Biogeosciences Discussions* 1–32. <https://doi.org/10.5194/bg-2020-323>.
- Yang, X., Tang, J.W., Mustard, J.F., Lee, J.E., Rossini, M., Joiner, J., Munger, J.W., Kornfeld, A., Richardson, A.D., 2015. Solar-induced chlorophyll fluorescence that correlates with canopy photosynthesis on diurnal and seasonal scales in a temperate deciduous forest. *Geophys. Res. Lett.* 42, 2977–2987. <https://doi.org/10.1002/2015gl063201>.
- Zeng, Y., Badgley, G., Dechant, B., Ryu, Y., Chen, M., Berry, J.A., 2019. A practical approach for estimating the escape ratio of near-infrared solar-induced chlorophyll fluorescence. *Remote Sensing of Environment*, 111209. <https://doi.org/10.1016/j.rse.2019.05.028>.
- Zhang, C., Filella, I., Garbulsky, M.F., Penuelas, J., 2016. Affecting Factors and Recent Improvements of the Photochemical Reflectance Index (PRI) for Remotely Sensing Foliar, Canopy and Ecosystemic Radiation-Use Efficiencies. *Remote Sens.* 8, 33. <https://doi.org/10.3390/rs8090677>.
- Zhang, Y.G., Guanter, L., Berry, J.A., van der Tol, C., Yang, X., Tang, J.W., Zhang, F.M., 2016. Model-based analysis of the relationship between sun-induced chlorophyll fluorescence and gross primary production for remote sensing applications. *Remote Sens. Environ.* 187, 145–155. <https://doi.org/10.1016/j.rse.2016.10.016>.
- Zhang, Z., Zhang, Y., Joiner, J., Migliavacca, M., 2018. Angle matters: Bidirectional effects impact the slope of relationship between gross primary productivity and sun-induced chlorophyll fluorescence from Orbiting Carbon Observatory-2 across biomes. *Global change biology* 24 (11), 5017–5020. <https://doi.org/10.1111/gcb.14427>.